2017-01-30

The Merlin tumour suppressor controls the repair capacity of Schwann cells following injury by regulating Hippo pathway signalling

Mindos, T

10.1083/jcb.201606052
Journal of Cell Biology
Rockefeller University Press

Published January 30, 2017

Merlin controls the repair capacity of Schwann cells after injury by regulating Hippo/YAP activity

Thomas Mindos,[1] Xin-peng Dun,[1] Katherine North,[1,5] Robin D.S. Doddrell,[1] Alexander Schulz,[2] Philip Edwards,[3] James Russell,[1] Bethany Gray,[1,5] Sheridan L. Roberts,[1] Aditya Shivane,[3] Georgina Mortimer,[1] Melissa Pirie,[1] Nailing Zhang,[4] Duojia Pan,[4] Helen Morrison,[2] and David B. Parkinson[1]

[1]Plymouth University Peninsula Schools of Medicine and Dentistry, Plymouth PL6 8BU, England, UK
[2]Leibniz Institute for Age Research – Fritz Lipmann Institute Jena, D-07745 Jena, Germany
[3]Department of Cellular and Anatomical Pathology, Derriford Hospital, Plymouth PL6 8DH, England, UK
[4]Department of Molecular Biology and Genetics, Howard Hughes Medical Institute, Johns Hopkins University School of Medicine, Baltimore, MD 21205
[5]University of Bath, Bath BA2 7AY, England, UK

Loss of the Merlin tumor suppressor and activation of the Hippo signaling pathway play major roles in the control of cell proliferation and tumorigenesis. We have identified completely novel roles for Merlin and the Hippo pathway effector Yes-associated protein (YAP) in the control of Schwann cell (SC) plasticity and peripheral nerve repair after injury. Injury to the peripheral nervous system (PNS) causes a dramatic shift in SC molecular phenotype and the generation of repair-competent SCs, which direct functional repair. We find that loss of Merlin in these cells causes a catastrophic failure of axonal regeneration and remyelination in the PNS. This effect is mediated by activation of YAP expression in Merlin-null SCs, and loss of YAP restores axonal regrowth and functional repair. This work identifies new mechanisms that control the regenerative potential of SCs and gives new insight into understanding the correct control of functional nerve repair in the PNS.

Introduction

Although the peripheral nervous system (PNS) may repair effectively after injury, such repair relies upon both the neurons and Schwann cells (SCs) to hugely change their roles from a function that supports normal nerve transmission to a function supporting repair and regeneration (Kim et al., 2013; Jessen et al., 2015; Jessen and Mirsky, 2016). The generation of repair-competent SCs distal to the site of the injury, termed Büngner cells, involves the transcription factor cJun-dependent loss of myelin proteins, recruitment of macrophages, and the activation of the specific repair program in SCs (Parkinson et al., 2008; Arthur-Farraj et al., 2012; Jessen and Mirsky, 2016). The slowed axonal regeneration that occurs in older mice is also associated with an impaired induction of cJun and reduced myelin clearance in SCs after injury (Kang and Lichtman, 2013; Painter et al., 2014). Injury to the PNS also triggers the activation of MAPK pathways within SCs, such as the extracellular regulated kinases (ERKs) 1/2 and p38 pathways, and signaling through these pathways regulates the dedifferentiation of SCs and immune cell entry into the nerve after injury (Harrisingh et al., 2004; Napoli et al., 2012; Yang et al., 2012).

The Merlin tumor suppressor has been well characterized for its roles in controlling cell signaling, contact-mediated inhibition of growth, and tumorigenesis. Loss of function of Merlin, either sporadically or in the inherited condition of neurofibromatosis type 2, leads to the formation of tumors within the nervous system, including schwannomas, meningiomas, and ependymomas in affected individuals (Hanemann, 2008; Hilton and Hanemann, 2014). Loss of Merlin leads to dysregulation of many cell processes, including control of the $CRL4^{DCAF1}$ E3 ubiquitin ligase, regulation of MAPK signaling, and a decrease in the Hippo signaling pathway, leading to increased activity of the Hippo effectors Yes-associated protein (YAP) and transcription coactivator with PDZ-binding motif (TAZ; Ammoun et al., 2008; Cooper and Giancotti, 2014).

Although much of the research has focused on the role of Merlin in schwannoma formation, many patients with NF2 also have a peripheral neuropathy, and it has been shown that expression of the Merlin isoform 2 within the neurons of the PNS is necessary for maintaining axonal integrity through maintaining correct neurofilament heavy chain phosphorylation (Schulz et al., 2013). More recently, axonal Merlin has also been shown to regulate neuregulin 1 type III expression on PNS axons and expression of the ErbB2 receptor on SCs (Schulz et al., 2014a). The combined axonal and SC heterozygosity for Merlin in patients with neurofibromatosis type 2 has also been

Correspondence to David B. Parkinson: david.parkinson@plymouth.ac.uk

Abbreviations used: ERK, extracellular regulated kinase; GDNF, glial cell line–derived neurotrophic factor; MBP, myelin basic protein; PNS, peripheral nervous system; PTEN, phosphatase and tensin homologue; SC, Schwann cell; SSI, static sciatic index; TAZ, transcription coactivator with PDZ-binding motif; YAP, Yes-associated protein.

The Rockefeller University Press $30.00
J. Cell Biol.
https://doi.org/10.1083/jcb.201606052

Published January 30, 2017

proposed as a likely contributor to potential tumor formation in the PNS (Schulz et al., 2016).

Although the generation of Merlin-null SC tumors, schwannomas, in the PNS has been well studied, the function of Merlin-dependent signaling in the processes and control of PNS regeneration and repair has not been fully investigated. Using a sciatic nerve crush model of nerve repair in mice with SC-specific deletion of Merlin, we found that Merlin function is crucial for the generation of the repair-competent SCs, which facilitate axonal regeneration and functional repair in the PNS. We observed significant increases in SC proliferation and macrophage infiltration in Merlin-null nerves, and a severely impaired axonal regeneration and remyelination, together with a reduced induction of cJun after injury. In addition to this, analysis of signaling in Merlin-null nerves after injury shows changes in MAPK signaling and a specific injury-dependent activation of YAP in Merlin-null SCs. We have further tested the significance of this altered Hippo pathway signaling and show, remarkably, that removal of YAP alone functionally corrects the PNS repair defects seen in Merlin-null nerves, restoring cJun and neurotrophin expression together with axonal regeneration and functional recovery after injury. These findings identify completely novel functions for both Merlin and the YAP protein in the regenerative capacity of the PNS and may point to potential new ways to boost PNS function and repair in diseases or after injury.

Results

Loss of Merlin in SCs causes a transient hypomyelination in the PNS

Little is known about the effects of Merlin loss upon the control of SC development and myelination, although previous studies in Merlin-conditional null animals have assessed the potential for schwannoma tumor development (Giovannini et al., 2000; Denisenko et al., 2008; Gehlhausen et al., 2015). Using the well-characterized mP_0TOTA-CRE (P0-CRE) line to specifically remove Merlin in SCs of the PNS at embryonic day 13.5 (Feltri et al., 1999), we first tested the roles of Merlin in controlling SC myelination and cell number. Analysis of myelination at postnatal day (P) 6 showed a hypomyelination of the sciatic nerve in mice with SC-specific loss of Merlin by both EM and Western blot analysis (Fig. 1, A, B, and E; and Fig. S1 D). Numbers of SCs were slightly but significantly raised in Merlin-null animals at both P6 and in adult animals (Figs. 1 F and S1, E–G), and, in confirmation of previous data (Denisenko et al., 2008), we also observed a shorter internodal distance together with increased numbers of Schmidt-Lanterman incisures in the peripheral nerves of Merlin-null animals at P60 (Fig. S5, H–M). Analysis of P21 and P60 nerves showed that by these later time points, however, myelination appeared normal with only small nonsignificant differences in myelin thickness (G ratio) between control and Merlin-null animals and comparable myelin protein expression (Figs. 1, C, D, and G; 2 M; 9 F; and S1, A–C). All measures of peripheral nerve function, such as nerve conduction velocity, compound muscle action potential, and functional testing of animals using a rotarod to check sensory–motor coordination, showed no significant differences between adult control and Merlin-null animals (Fig. 5, E–G; and Fig. S5 G).

Loss of Merlin in SCs causes a failure of regeneration and remyelination after injury

Injury to the PNS starts a series of well-characterized events distal to the site of the injury that include the degeneration of axons, immune cell infiltration, and reprogramming of SCs to assume a repair-competent state (Arthur-Farraj et al., 2012; Kim et al., 2013; Jessen and Mirsky, 2016). As Merlin is a key regulator of cell signaling, we analyzed the control of repair after crush injury in the sciatic nerve with SC-specific deletion of Merlin.

For Merlin-null nerves, we observed a large decrease in the numbers of regenerating axons and almost no remyelination as compared with controls (Fig. 2, C–L). We also observed a significant expansion of the entire nerve distal to the site of injury (Fig. 2, A, B, and G–J). Corresponding to the lack of remyelination, Western blotting for myelin basic protein (MBP) showed almost undetectable levels in Merlin-null distal nerves at 21 d after injury, but MBP was reexpressed in control nerves, demonstrating the onset of remyelination in these animals (Fig. 2 M). Even at 60 d after crush injury, axonal regeneration and remyelination were both very poor in Merlin-null nerves as compared with controls (Fig. 2, I, J, and L).

Numbers of regenerated axons within the tibial nerve showed a large reduction in Merlin-null animals at both 21 and 60 d after injury, and those axons that did regenerate associated poorly with SCs (Fig. 3, A–F). Even when larger diameter axons regenerated into the distal tibial Merlin-null nerve, they were poorly myelinated, with increased G ratios at both 21 and 60 d after crush injury (Fig. 3, G and H). After injury, we also observed greatly increased numbers of SCs, which displayed extensive cellular processes; many SCs ensheathed groups of collagen fibers (Fig. 3, B, D, I, and J). Even when correctly associating with and myelinating an axon, Merlin-null SCs exhibited the same multiple cell processes and discontinuous basal lamina (Fig. 3 I). To test whether this SC behavior within the Merlin-null distal nerve may be caused by the lack of regenerating axons, we performed experiments in which a section of the nerve was removed to prevent axonal regeneration into the distal stump. We never observed such SC behavior or collagen wrapping in control animals, even at 60 d after injury (unpublished data), indicating that this effect was specific to nerves containing Merlin-null SCs and not an effect of the continued absence of axons within the nerve distal to the crush site.

We next extended this analysis to an even longer time point of 8 mo after crush injury. Remarkably, even at this time, analysis of distal nerve samples from Merlin-null animals still showed a lack of axonal regeneration and remyelination, demonstrating that the regeneration defect does not correct in nerves containing Merlin-null SCs (Fig. S2, A–H). Staining with Masson's trichrome stain also revealed the large amount of collagen within the injured Merlin-null nerves at this time point (Fig. S2, I and J). Together, these findings show a crucial role for the Merlin in SCs to generate the repair-competent Büngner cells required for efficient axonal regeneration and remyelination after injury to the PNS.

Reduced axonal regeneration and elevated cell proliferation, together with increased and sustained macrophage numbers in Merlin-null nerves after injury

We have previously described the use of wholemount staining to visualize axonal regeneration after both cut and crush injuries (Dun and Parkinson, 2015). Using this technique, we saw that

Published January 30, 2017

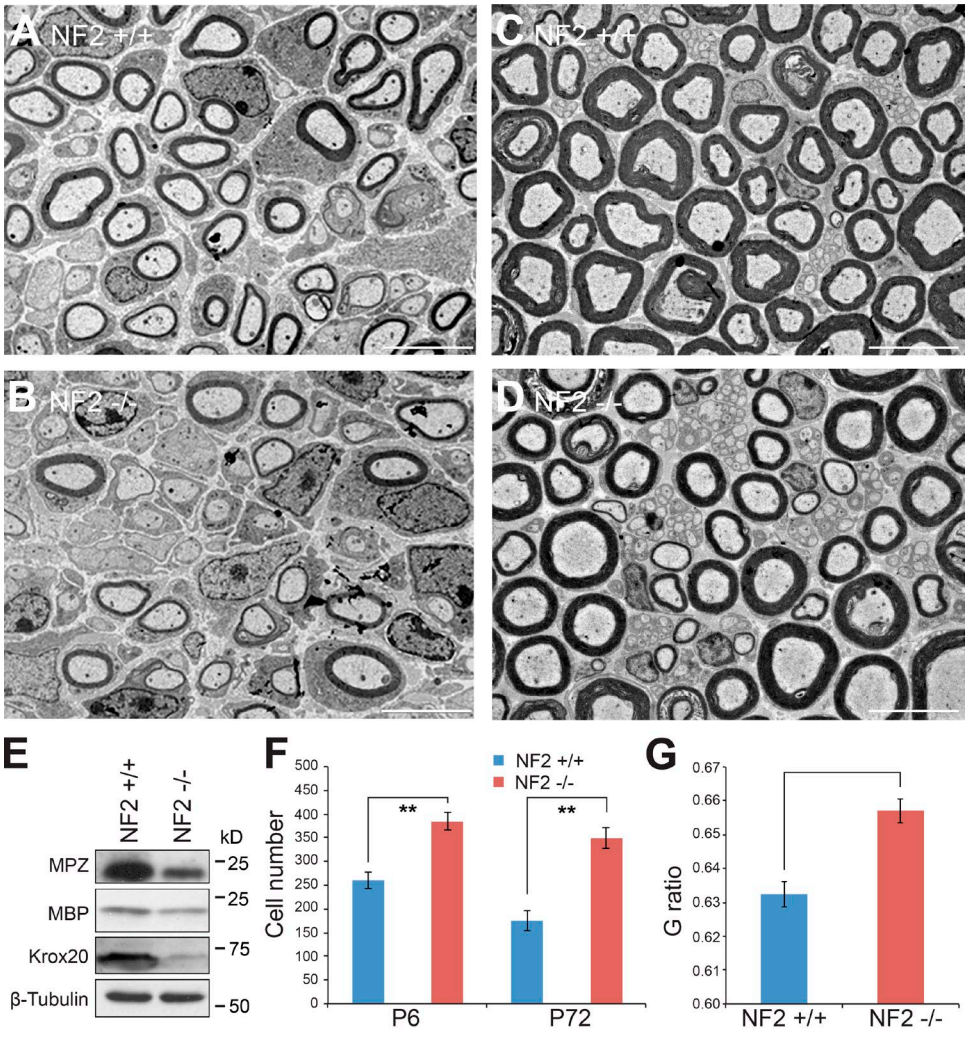

Figure 1. **Merlin-null nerves show a transient hypomyelination and slight increase in SC numbers.** (A and B) Transmission EM pictures of P6 sciatic nerves from control ($NF2^{+/+}$) and Merlin-null ($NF2^{-/-}$) animals. (C and D) Transmission EM pictures of P60 sciatic nerves from control (C) and Merlin-null (D) animals. (A–D) n = 3 mice. Bars, 10 µm. (E). Western blot of control and Merlin-null nerves at P6. n = 3 pools; 1 pool = 3 nerves from three mice for each genotype. β-Tubulin was used as a loading control. (F) Counts of Hoechst-stained nuclei from transverse cryostat sections of P6 and P72 sciatic nerves showing increases in cell number in Merlin-null nerves. For $NF2^{+/+}$, n = 3; for $NF2^{-/-}$, n = 4. (G) Small but nonsignificant increase in G ratio in P60 Merlin-null nerves as compared with control. n = 3 mice. (F and G) Two-sided two-sample Student's t test: **, $P \leq 0.004$ (P6; F); **, $P \leq 0.005$ (P72; F); $P = 0.1$ (G). Data are presented as means ± SEM.

the distance of the leading regenerating axon was significantly reduced in Merlin-null nerves at 7 d after crush injury (Fig. 4, A–C). Using neurofilament staining to identify regenerating axons in transverse sections of sciatic nerve distal to the injury site, there was a clear reduction in the numbers of regenerating axons in the distal sciatic nerve at both 7 and 21 d after crush injury in Merlin-null nerves (Fig. 4, D–G).

Injury to peripheral nerves induces distal SC demyelination and proliferation, breakdown of the blood–nerve barrier, and consequent macrophage influx to the nerve (Jessen and Mirsky, 2016). We found that after crush injury at 7 d, both proliferation, measured by Ki67 labeling (Fig. 4 H), and macrophage numbers, measured by Iba1/F4/80 double labeling (Iba1 staining shown), were significantly elevated in Merlin-null nerves. Even at later time points, 21 and 60 d after injury, significantly more macrophages were present within Merlin-null nerves (Fig. 4, I–K), demonstrating an ongoing inflammatory response in these animals.

Loss of functional recovery in Merlin-null nerves

Next, we used several measurements to assess functional recovery in Merlin-null nerves after injury. After a sciatic nerve crush injury, control animals recover function fully by 21 d, as previously reported (Fig. 5 A; Yang et al., 2008; Arthur-Farraj et al., 2012), and our analysis of the tibial nerves from control animals show normal axonal regeneration and remyelination at this time point (Fig. 2 G). Assessment of functional recovery by the static sciatic index (SSI), a gait analysis which measures sensory–motor recovery (Baptista et al., 2007), showed no functional recovery at 21 d in Merlin-null animals as compared with a full recovery by control animals using this test (Fig. 5 A). Analysis of functional recovery using single-frame motion analysis of both foot–base angle and lateral foot–base angle to measure recovery of motor function (Fey et al., 2010) showed significant deficits in function in Merlin-null animals at 35 d and foot–base angle at 105 d after injury,

Published January 30, 2017

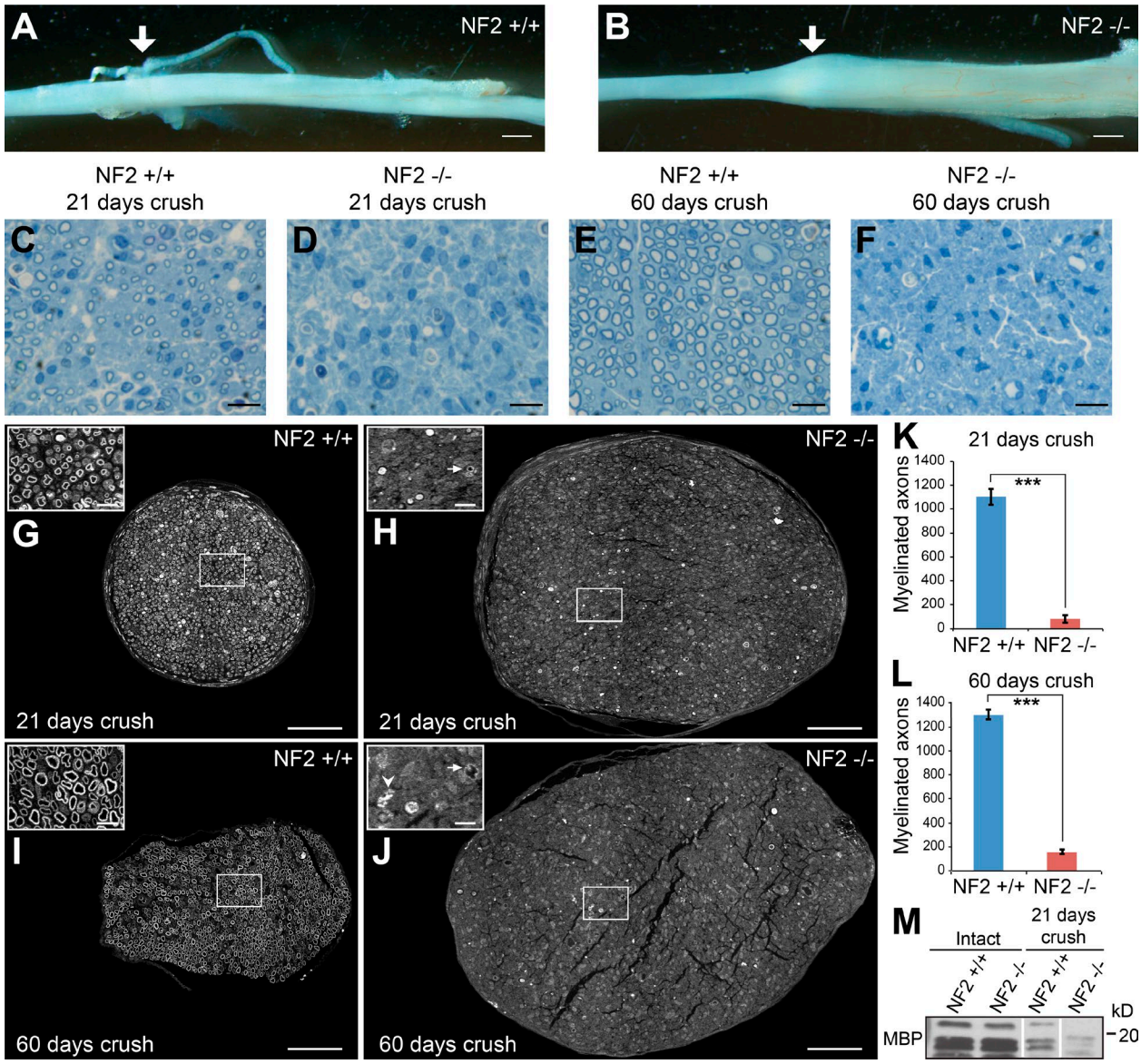

Figure 2. **Loss of Merlin in SCs causes a severe regeneration defect after injury.** (A and B) Phase photos showing the sciatic nerve 21 d after crush injury in control ($NF2^{+/+}$) and SC-specific Merlin-null ($NF2^{-/-}$) nerves; the white arrows mark the site of crush injury. There is a substantial expansion of the distal nerve in Merlin-null nerves (observed in all analyzed $NF2^{-/-}$ nerves after injury). Bars, 2 mm. (C–F) Semithin sections of the distal sciatic nerve at 21 (C and D) and 60 d (E and F) after crush injury. (G–J) Low-vacuum scanning EM of control (G and I) and Merlin-null (H and J) tibial nerves at 21 and 60 d after crush injury; insets show higher magnification images of the samples, showing remyelination in control samples but almost no remyelination in Merlin-null nerves. Arrows in insets in H and J show thinly remyelinated axons. The arrowhead in the inset in J shows the presence of macrophages in the nerve at 60 d. Bars: 50 µm (main images); 25 µm (insets). (K and L) Counts of numbers of myelinated fibers in tibial nerves at 21 and 60 d after crush injury with significantly fewer myelinated fibers in $NF2^{-/-}$ nerves at both time points. Two-sided two-sample Student's *t* test: ***, $P \leq 0.001$ in both time points. Data are presented as means ± SEM. (M) Western blot of MBP in intact and injured distal sciatic nerves 21 d after nerve crush. White lines indicate that intervening lanes have been spliced out. (G–M) $n = 3$ mice for each genotype and time point.

confirming the long-term loss of nerve function in these animals (Fig. 5, B–D). Furthermore, measurements of both nerve conduction velocity and compound muscle action potential, to assess axon regeneration, reinnervation, and remyelination in nerves 35 d after crush injury, showed significant reductions in Merlin-null animals (Fig. 5, E–G). Measures of the recovery of sensory function in the foot by the toe pinch test also showed little or no recovery even at 35 d in Merlin-null animals as compared with control animals that showed full recovery at 21 d (Fig. S3).

Alterations in Hippo pathway signaling, cJun expression, and MAPK activation in Merlin-null nerves after injury

The poor axonal regeneration seen in Merlin-null animals partly resembles that seen in animals with SC-specific loss of the transcription factor cJun, although there are also clear differences in phenotype between these two transgenic lines; for instance, the increased macrophage infiltration seen in Merlin-null nerves is not seen in cJun-null nerves after injury (Arthur-Farraj et al., 2012).

Published January 30, 2017

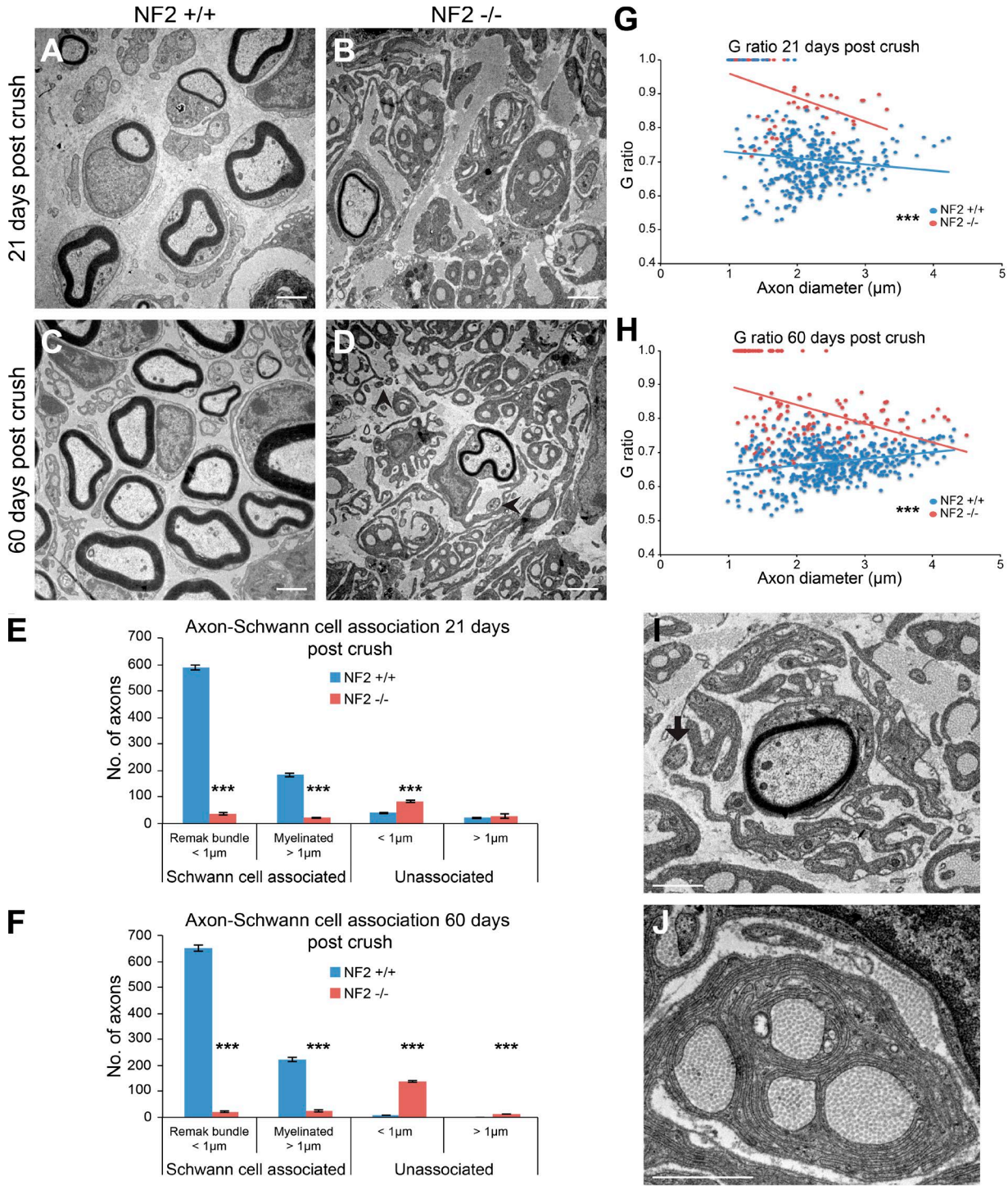

Figure 3. **Remyelination and morphological analysis of control and Merlin-null nerves after injury.** (A–D) Transmission EM pictures of control ($NF2^{+/+}$) and Merlin-null ($NF2^{-/-}$) distal sciatic nerves at 21 and 60 d after nerve crush. Black arrowheads in D indicate small-diameter axons that are unassociated with SCs. *n* = 3 mice. Bars, 2 µm. (E and F) Counts of axons and axon–SC association in sciatic nerves of control and Merlin-null animals at 21 and 60 d after injury, indicating poor association of Merlin-null SCs with both small-diameter (<1 µm) and larger-diameter (>1 µm) axons and corresponding increased numbers of unassociated axons in these nerves after injury. *n* = 3 mice. Data are presented as means ± SEM. (G and H) G ratio versus axon diameter scatter plot graphs for control and Merlin-null sciatic nerves at 21 and 60 d after injury. *n* = 3 mice. (E–H) Two-sided two-sample Student's *t* test: ***, $P \leq 0.001$ for all comparisons in axon–SC association graphs against the control $NF2^{+/+}$ at both time points E and F; $P = 0.464$ for unassociated axons >1 µm (E); and ***, $P \leq 0.001$ for the G ratio at 21 and 60 d after crush (G and H). (I and J) Transmission EM of Merlin-null sciatic nerves at 60 d after crush injury showing large amounts of collagen fibers, extensive SC processes, and a large degree of collagen wrapping by SCs within the nerve. The black arrow in I indicates a small-diameter axon that is unassociated with an SC and is residing inside the discontinuous basal lamina of the myelinating SC. Notice in J that the SC ensheaths the collagen fibers with multiple membrane bilayers. Representative images from three biological replicates are shown. Bars, 1 µm.

Published January 30, 2017

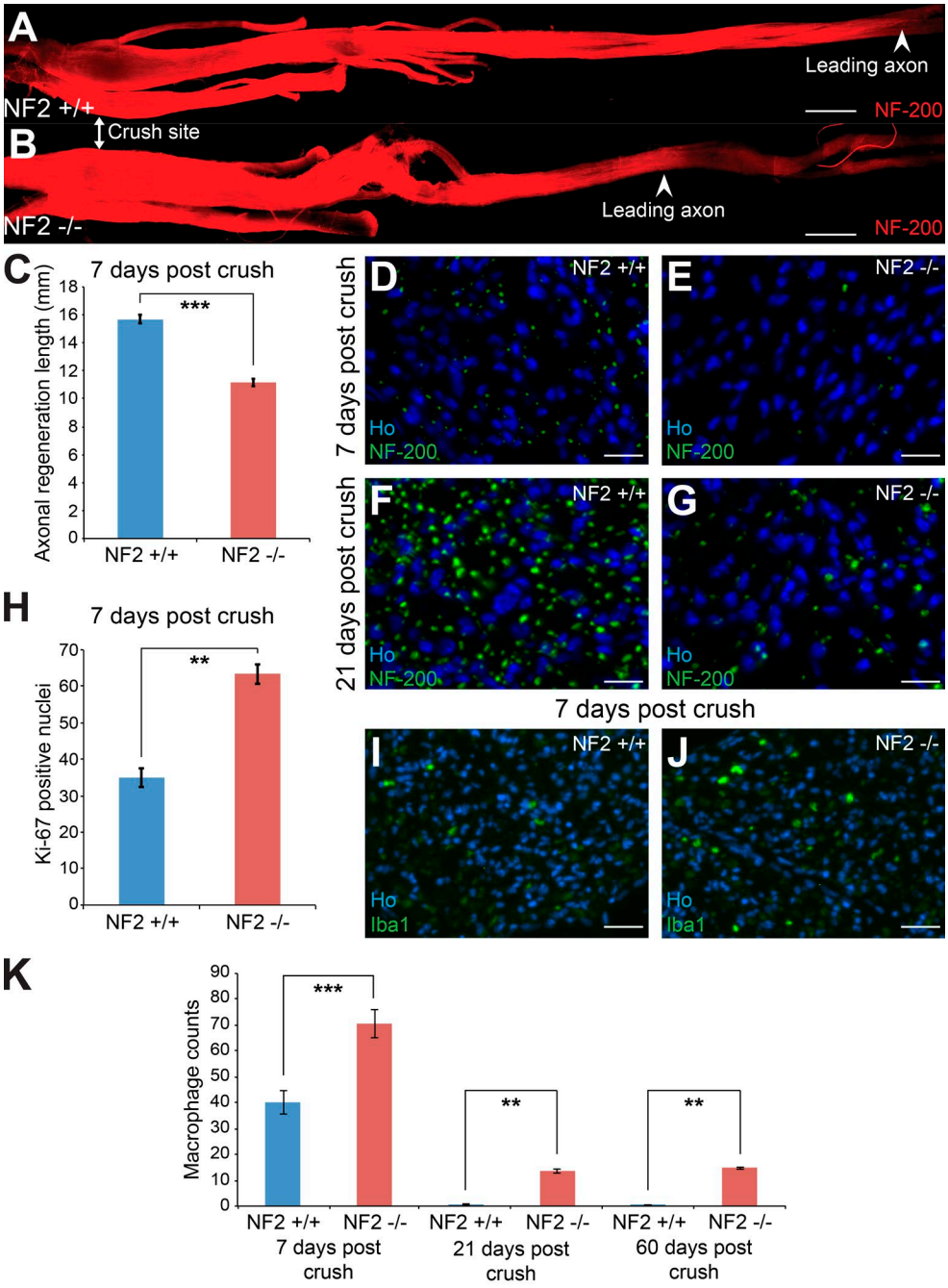

Figure 4. **Loss of Merlin causes a failure in axonal regrowth, and distal nerves are characterized by increased SC proliferation and the ongoing presence of macrophages.** (A and B) Wholemount staining of control ($NF2^{+/+}$) and Merlin-null ($NF2^{-/-}$) nerves at 7 d after crush injury. Nerves were stained with neurofilament antibody (NF200). The crush site is marked, and arrowheads mark the leading regenerating axons in control and Merlin-null nerves. Bars, 1 mm. (C) Quantification of the distance of leading axons relative to injury site at 7 d after crush in control and Merlin-null nerves. (D–G) Immunolabeling with neurofilament antibody of the distal sciatic nerve at 7 and 21 d after nerve crush. Bars, 25 µm. (H) Increased SC proliferation, as measured by Ki67 labeling, in a Merlin-null distal sciatic nerve at 7 d after crush injury. (C–H) $n = 3$ mice. (I–K) Labeling (I and J) and quantification (K) of Iba1-positive macrophages in control and Merlin-null sciatic nerves at 7, 21, and 60 d after crush injury. $n = 3$ mice for each genotype and time point. Bars, 100 µm. Data are presented as means ± SEM. (C, H, and K) Two-sided two-sample Student's *t* test: **, $P \leq 0.01$; ***, $P \leq 0.001$.

Measurement of cJun protein levels in Merlin-null nerves showed a reduced induction of cJun protein at 4, 7, and 11 d after crush injury (Fig. 6, A, B, and D) and at 7 d after cut injury (Fig. 6 C) in Merlin-null animals by both immunolabeling and Western blotting. In the nerve crush experiments, as cJun levels began to drop at 21 d after crush injury in control animals, presumably reflecting the remyelination of the distal nerve, weak cJun expression was maintained in Merlin-null animals at this time point, underlining the lack of remyelination seen (Fig. 2, H and M; and Fig. 9 F). In keeping with this effect and with the lack of remyelination in Merlin-null animals, we observed increased levels of the immature SC marker N-cadherin in Merlin-null animals at later time points after injury and reduced levels of E-cadherin (Fig. 6 D); E-cadherin

Published January 30, 2017

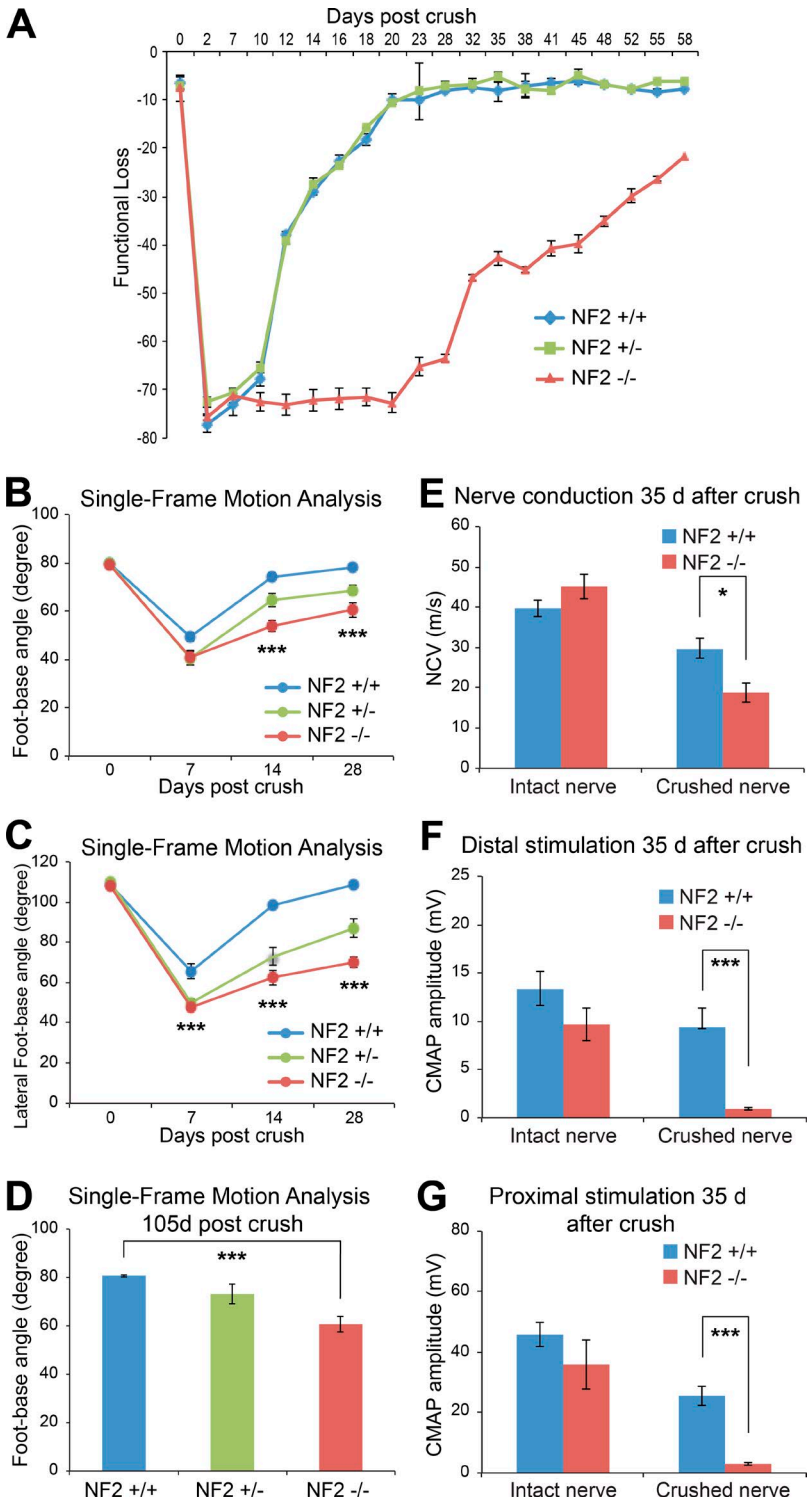

Figure 5. **Merlin-null animals display diminished functional recovery at all time points after injury.** (A) SSI measurements of control ($NF2^{+/+}$), heterozygous ($NF2^{+/-}$), and Merlin-null animals ($NF2^{-/-}$). $n = 3$ mice for each time point. (B and C) Single-frame motion analysis of animals for foot–base angle and lateral foot–base angle up to 28 d after crush injury. (D) Measurement of foot–base angle in animals at 15 wk (105 d) after crush injury. $n = 7$ mice for each time point. (B–D) One-way analysis of variance with Bonferroni's multiple comparison test: ***, $P \leq 0.001$ for all time points compared with $NF2^{+/+}$. (E) Measurements of nerve conduction velocity (NCV) of control and Merlin-null animals from contralateral control and side of nerve crush at 35 d after crush injury. (F and G) Measurements of compound muscle action potential (CMAP) with distal and proximal stimulation. Data are presented as means ± SEM. (E–G) $n = 7$ mice. (E–G) Two-sided two-sample Student's *t* test: *, $P = 0.014$; ***, $P \leq 0.001$.

is induced in SCs as they begin to myelinate (Crawford et al., 2008). In addition, we saw increased levels of active β-catenin in Merlin-null nerves after injury.

Although we observed reduced levels of cJun in Merlin-null SCs after injury, we did not observe in vitro nor in vivo the delayed dedifferentiation and loss of myelin proteins seen in cJun-null animals at 7 d after nerve cut injury (Fig. 6 C and not depicted).

Induction of the SC chemokine monocyte chemoattractant protein 1, MCP1/CCL2, is known to be important for entry of macrophages into the nerve after injury and is regulated by activity of the MEK/ERK1/2 pathway in SCs; in addition, activation of the p38 MAPK pathway has been implicated in macrophage recruitment and activation after injury (Tofaris et al., 2002; Myers et al., 2003; Fischer et al., 2008a; Napoli et al., 2012). Activity of both the ERK1/2 and p38 MAPK pathways were elevated in Merlin-null nerves after both crush and cut injury, as well as levels of MCP1 protein (Fig. 6, C and D), in accordance with the increased numbers and persistent presence of macrophages within the Merlin-null nerves after injury (Fig. 4, I–K).

Published January 30, 2017

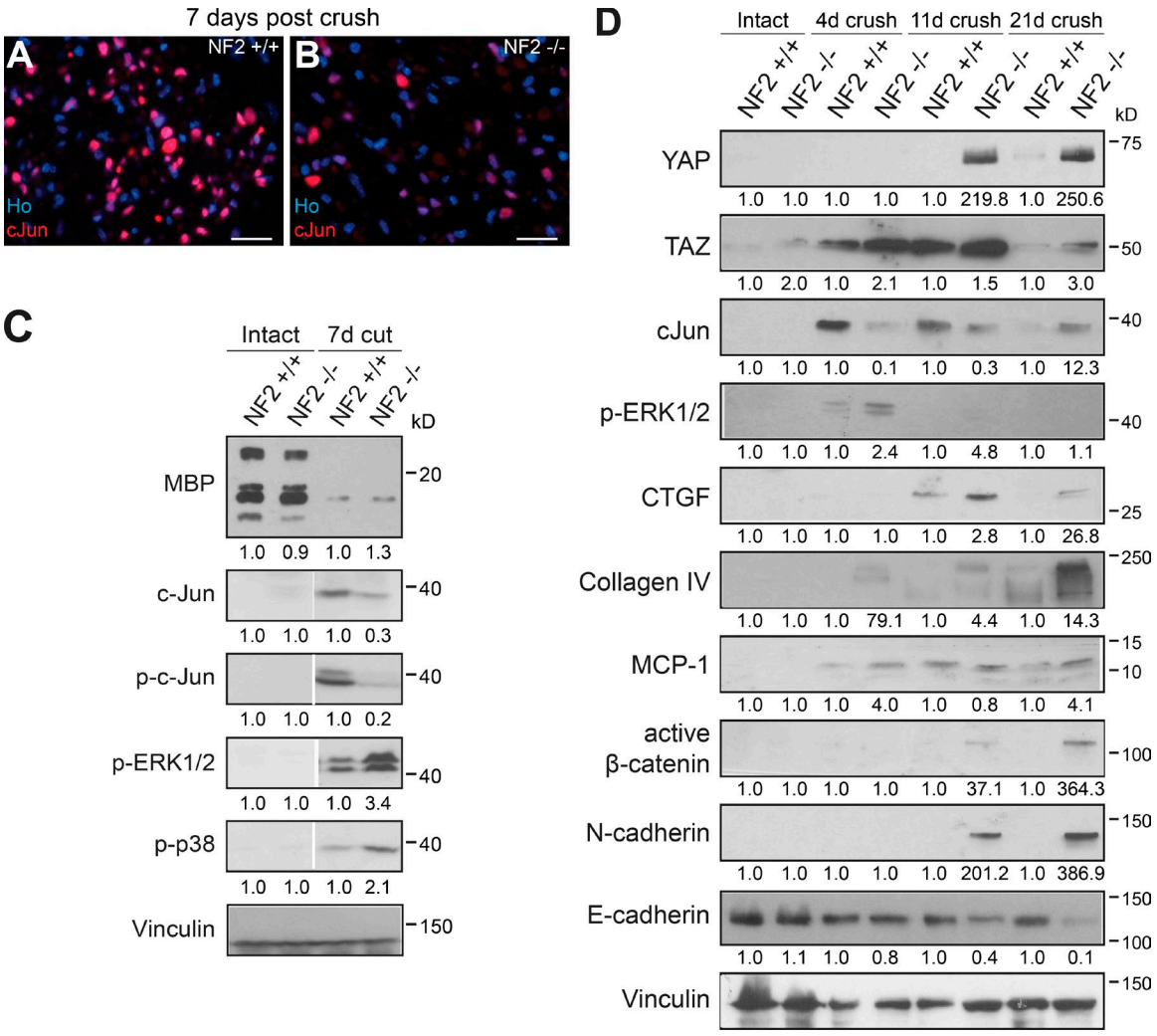

Figure 6. **Merlin function in SCs regulates cJun expression together with MAPK and Hippo pathway signaling after injury.** (A and B) Immunolabeling of the distal sciatic nerve in control ($NF2^{+/+}$) and Merlin-null ($NF2^{-/-}$) sciatic nerves 7 d after nerve crush injury with cJun antibody. *n* = 3 mice. Bars, 25 µm. (C) Western blot of intact and injured distal sciatic nerves 7 d after nerve cut injury in control and Merlin-null nerves. *n* = 3 pools; 1 pool = 3 nerves from three mice for each genotype. Values represent normalized expression against the control for each time point. Vinculin is used as a loading control. White lines indicate that intervening lanes have been spliced out. (D) Western blots of distal control and Merlin-null nerves at 4, 11, and 21 d after nerve crush injury. *n* = 3 pools; 1 pool = 3 nerves from three mice for each genotype. Values represent normalized expression against the control for each time point. Vinculin is used a loading control. CTGF, connective tissue growth factor.

The failure of Merlin-null nerves to repair is dependent on activation of the Hippo pathway effector YAP

A key function of the Merlin tumor suppressor in cells is to regulate activity of the Hippo pathway. The Hippo pathway effectors YAP and TAZ are phosphorylated by the LATS1/2 kinases, which inactivates their function by increasing YAP/TAZ retention in the cytoplasm (Cooper and Giancotti, 2014). Loss of Merlin in tumor cells leads to increased YAP/TAZ-dependent signaling, and the formation of Merlin-null liver tumors requires YAP function (Zhang et al., 2010). Western blotting of distal nerve samples after injury showed an increase in YAP levels only in Merlin-null nerves after injury, whereas for TAZ we saw an increase in levels in both control and Merlin-null animals, albeit at higher levels in the Merlin-null animals (Fig. 6 D). The level of connective tissue growth factor, which is a Hippo target (Zhao et al., 2010; Shimomura et al., 2014), was also strongly increased, together with raised levels of collagen type IV in Merlin-null nerves after injury (Fig. 6 D).

Given the strong injury-specific activation of YAP in Merlin-null nerves, we next tested the effects of removing YAP function in SCs. Mice with a conditional allele of the YAP locus (Zhang et al., 2010), $YAP^{fl/fl}$, were crossed with Merlin-conditional animals, $NF2^{fl/fl}$, to generate Merlin-null animals with the loss of either one ($NF2^{-/-}YAP^{+/-}$) or both ($NF2^{-/-}YAP^{-/-}$) YAP alleles. Analysis of mice with an SC-specific deletion of YAP alone ($NF2^{+/+}YAP^{-/-}$) revealed no developmental abnormalities in the nerve as measured by transmission EM of the sciatic nerve at P6 and P21 (Fig. S4, A–E), and injury experiments in these animals showed a recovery profile, as measured by SSI analysis, indistinguishable from control wild-type animals (Fig. S4 G). Proliferation after injury at 7 d showed no change in the numbers of Ki67-positive proliferating SCs or numbers of Iba1-positive macrophages recruited to the nerve in $YAP^{-/-}$ single-null animals (Fig. S4, F and H). Both $NF2^{-/-}YAP^{+/-}$ and $NF2^{-/-}YAP^{-/-}$ animals were phenotypically normal, and analysis of the adult intact nerve in these animals revealed no abnormalities in axon number, diameter, or myelination by G ratio analysis and Western blotting

Published January 30, 2017

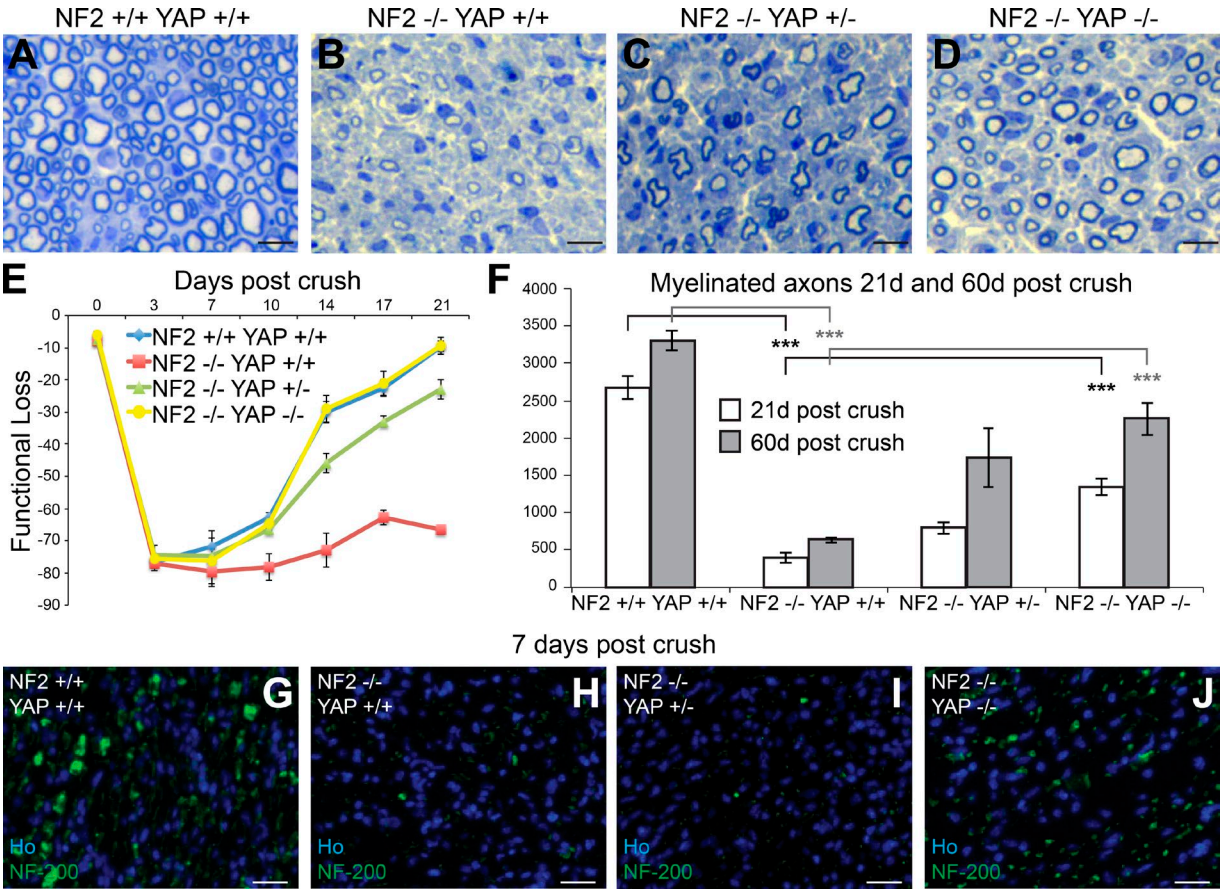

Figure 7. **Loss of YAP in Merlin-null SCs improves both axonal repair and functional recovery after injury.** (A–D) Toluidine blue–stained semithin sections of the distal sciatic nerve at 60 d after crush injury showing increased numbers of myelinated axons in NF2$^{-/-}$YAP$^{-/-}$ double-null nerves (D) compared with NF2$^{-/-}$YAP$^{+/+}$ Merlin single-null animals (B). Mice with loss of one YAP allele (NF2$^{-/-}$YAP$^{+/-}$; C) have an intermediate phenotype. *n* = 3 mice for all genotypes. Bars, 10 µm. (E) SSI analysis of control, Merlin single-null, and Merlin/YAP double-null animals. *n* = 3 mice for each experiment and time point. (F) Counts of myelinated axons in the distal sciatic nerve of control, single Merlin-null, and Merlin/YAP double-null animals at 21 d (*n* = 6 for each genotype and time point) and 60 d (*n* = 3 mice for each genotype and time point) after crush injury. (F) One-way analysis of variance with Bonferroni's multiple comparison test: ***, $P \leq 0.001$ in the comparisons shown. Data are presented as means ± SEM. (G–J) Immunolabeling of the distal sciatic nerve with neurofilament antibody in control, single Merlin-null, and Merlin/YAP double-null animals 7 d after crush injury. *n* = 3 mice. Bars, 50 µm.

(Figs. 9 F and S5, A–F). Functional testing of mice by rotarod analysis showed no differences between adult NF2$^{+/+}$YAP$^{+/+}$, NF2$^{-/-}$YAP$^{+/+}$, and NF2$^{-/-}$YAP$^{-/-}$ animals (Fig. S5 G).

As described in the first section of the Results and in a previous study (Denisenko et al., 2008), loss of Merlin in SCs causes both a shortening of the internodal distance in the adult nerve, increased numbers of SCs, and increased numbers of Schmidt-Lanterman incisures within myelinated SCs. Analysis of NF2$^{-/-}$YAP$^{+/-}$ and NF2$^{-/-}$YAP$^{-/-}$ adult P60 nerves showed that these three phenotypes were all corrected by the loss of YAP function in intact adult Merlin-null nerves (Fig. S5, L–N.)

Western blotting of NF2$^{+/+}$YAP$^{+/+}$, NF2$^{-/-}$YAP$^{+/+}$, and NF2$^{-/-}$YAP$^{-/-}$ nerves at 11 d after crush injury showed the loss of YAP induction in NF2$^{-/-}$YAP$^{-/-}$ animals, confirming the SC specificity of YAP induction in Merlin-null (NF2$^{-/-}$YAP$^{+/+}$) nerves after injury (Fig. 8 G).

Next, we performed sciatic nerve crush injury experiments and assessment of recovery in NF2$^{+/+}$YAP$^{+/+}$, NF2$^{-/-}$YAP$^{+/+}$, NF2$^{-/-}$YAP$^{+/-}$, and NF2$^{-/-}$YAP$^{-/-}$ animals.

Remarkably, loss of even one copy of YAP in the NF2$^{-/-}$YAP$^{+/-}$ animals was sufficient to restore some axonal regeneration and remyelination compared with the Merlin-null (NF2$^{-/-}$YAP$^{+/+}$) animals at 21 d after crush injury. Loss of the second YAP allele in NF2$^{-/-}$YAP$^{-/-}$ animals further restored axonal regeneration and numbers of myelinated fibers within the distal nerve (Fig. 7, A–D and F). Neurofilament staining in the distal sciatic nerve at 7 d after crush injury showed increased numbers of regenerating axons in both NF2$^{-/-}$YAP$^{+/-}$ and NF2$^{-/-}$YAP$^{-/-}$ animals as compared with NF2$^{-/-}$YAP$^{+/+}$ animals even at this early time point after injury (Fig. 7, G–J). At 60 d, there was a further improvement of regeneration in NF2$^{-/-}$YAP$^{-/-}$ animals compared with 21 d, with larger numbers of myelinated axons present within the distal sciatic nerve (Fig. 7 F).

As described in the Loss of functional recovery in Merlin-null nerves section, mice with SC-specific loss of Merlin failed to recover by 21 d as measured by SSI analysis (Fig. 5 A). In accordance with the axon regeneration and numbers of myelinated fibers in the distal nerve, loss of even one YAP allele in NF2$^{-/-}$YAP$^{+/-}$ animals almost completely restored functional recovery by this measure in animals at 21 d; loss of the second YAP allele (NF2$^{-/-}$YAP$^{-/-}$) led to a complete functional recovery at 21 d by SSI analysis with a recovery profile indistinguishable from the control NF2$^{+/+}$YAP$^{+/+}$ animals (Fig. 7 E). Sensory recovery, as measured by the toe pinch test, showed a slight delay, but all NF2$^{-/-}$YAP$^{-/-}$ animals showed a full recovery by this test at 26 d compared with 21 d for control animals. Transmission

Published January 30, 2017

EM showed increased myelin thickness and decreased G ratios for regenerated axons in the $NF2^{-/-}YAP^{+/-}$ and $NF2^{-/-}YAP^{-/-}$ animals as compared with Merlin-null ($NF2^{-/-}YAP^{+/+}$) nerves at 21 d after injury (Fig. 8, A–D, H, and I).

However, it should be noted that whereas there is a restoration of axonal regeneration, remyelination, and functional recovery with the loss of YAP in Merlin-null SCs, we still observed some, but reduced, numbers of abnormalities, such as increased numbers of collagen fibers, collagen wrapping by SCs, and large numbers of SC processes within $NF2^{-/-}YAP^{-/-}$ distal nerves at 21 d after injury (Fig. 8, D–F).

Next, we examined the role of YAP in the increased SC proliferation and macrophage infiltration seen in Merlin-null nerves after nerve crush injury (Fig. 4, H–K). We found that loss of YAP reduced both the elevated cell proliferation and macrophage influx seen in Merlin-null animals to that seen in control ($NF2^{+/+}YAP^{+/+}$) animals at 7 d after injury (Fig. 8, J and K); these findings once again underline the importance of YAP signaling on the phenotype observed in Merlin-null animals.

cJun and neurotrophin expression are reduced in Merlin-null nerves after injury in a YAP-dependent manner

The analysis of mice with SC-specific deletion of cJun has previously identified a reduced expression of the neurotrophins brain-derived neurotrophic factor, glial cell line–derived neurotrophic factor (GDNF), and artemin; administration of GDNF or artemin was shown to significantly improve the axon regeneration defect in cJun-null animals (Arthur-Farraj et al., 2012; Fontana et al., 2012). Given that we observed a reduced induction of cJun in Merlin-null nerves, we tested for mRNA and protein levels of cJun and of these neurotrophins after injury. At 4 d after crush injury, we observed a significant reduction in mRNA levels for cJun, brain-derived neurotrophic factor, GDNF, and artemin in Merlin-null nerves as compared with controls. In all cases, these changes were partially reversed in Merlin/YAP double-null animals (Fig. 9, A–D). These findings clearly identify for the first time that Merlin either directly or indirectly controls cJun expression in vivo in SCs after injury in a YAP-dependent manner. The partial restoration of cJun expression together with the reduction in ERK1/2 activation after injury in Merlin/YAP double-null animals was also confirmed by Western blotting (Fig. 9 E). In addition, an increase in TAZ protein was also observed in Merlin/YAP double-null nerves after injury (Figs. 8 G and 9 E). In keeping with the normalized macrophage numbers seen in Merlin/YAP double-null nerves after injury (Fig. 8 K), lower levels of MCP1 were observed in these nerves compared with Merlin-null nerves (Fig. 9 E).

Finally, to check the direct relationship between YAP expression and cJun expression, rat SCs were infected with adenovirus expressing either LacZ as a control or the non-phosphorylatable constitutively active FLAG-tagged $YAP^{Ser127Ala}$ (Shao et al., 2014), and levels of cJun protein were measured. Immunolabeling of infected SCs showed both nuclear and cytoplasmic localization of the $YAP^{Ser127Ala}$ protein (Figs. 9 I and S5, O and P). We found that expression of $YAP^{Ser127Ala}$ alone was sufficient to lower cJun protein levels in rat SCs (Fig. 9, G–J).

These findings clearly identify that after PNS injury, Merlin-dependent signaling controls the correct up-regulation of cJun in SCs, together with neurotrophin expression, to ensure efficient axonal regeneration and functional repair. Loss of Merlin and consequent activation of YAP function in SCs suppresses this part of the regenerative response, leading to a failure of repair in the nerve after injury.

Discussion

We have examined the consequences of Merlin loss upon the regenerative capacity of SCs in the PNS after injury. In this system, SCs adopt, by cellular reprogramming, a repair-specific phenotype after injury that is required for the full axonal regeneration and the functional repair that can occur in this tissue (Arthur-Farraj et al., 2012; Jessen et al., 2015; Jessen and Mirsky, 2016). Given the multiple functions of the Merlin protein, it was somewhat surprising that loss of Merlin in SCs developmentally has only minor consequences in the development of the postnatal and adult nerve, but, highlighting the potential differences between development and repair in the PNS, loss of Merlin in SCs causes the almost complete failure of repair after injury.

After injury in Merlin-null nerves, we observed an increase in SC proliferation, an inhibition of axonal regeneration, and a failure of SCs to correctly remyelinate the few large-diameter axons that do regenerate. In addition to this, we observed an ongoing inflammatory state with increased numbers of macrophages within the nerve. It is interesting that these features are also characteristic of human schwannoma tumors in patients with NF2 (de Vries et al., 2013), and the possibility of local nerve compression or small injury as a trigger for such tumor formation is possibly consistent with the sites of such tumors on the eighth cranial nerve and at the spinal nerve roots of the PNS (Asthagiri et al., 2009; Hilton and Hanemann, 2014). Our analysis of the histology of distal Merlin-null nerves at either 60 d or 8 mo after injury indicates that they do show similarities to cellular schwannomas, but we have not observed the hallmark signs of human schwannoma such as Antoni type A or B regions or Verocay bodies in our experiments (Fig. S2, K and L; not depicted; Hilton and Hanemann, 2014).

Previous work in both transgenic knockout and older animals has identified the cJun transcription factor as a key protein in the generation of the repair-competent SC, or Büngner cell, in the distal nerve after injury (Parkinson et al., 2008; Arthur-Farraj et al., 2012; Painter et al., 2014), and we found that the up-regulation of cJun is delayed in Merlin-null nerves; however, we did not observe the block in myelin protein down-regulation or the reduced recruitment of macrophages seen in cJun-null animals. It is unclear as to how much of a role this lack of myelin clearance plays in the reduced axonal regeneration seen in the cJun-null nerves, but other work has shown that increased myelin debris seen after injury in aged animals causes stalling of motor axon regrowth in the PNS (Kang and Lichtman, 2013). The apparently normal myelin clearance we observed in Merlin-null nerves would seemingly exclude this as a reason for the very poor regeneration of axons in our experiments. This, together with the altered cell proliferation and immune response we observed, highlights clear differences between the SC cJun and Merlin-null phenotypes after injury.

One possible explanation for the normal myelin clearance in Merlin-null nerves is that we also observed increased activation of both ERK1/2 and p38 pathways after injury in Merlin-null animals; both pathways have been shown to regulate SC demyelination and macrophage recruitment, and it is unclear

Published January 30, 2017

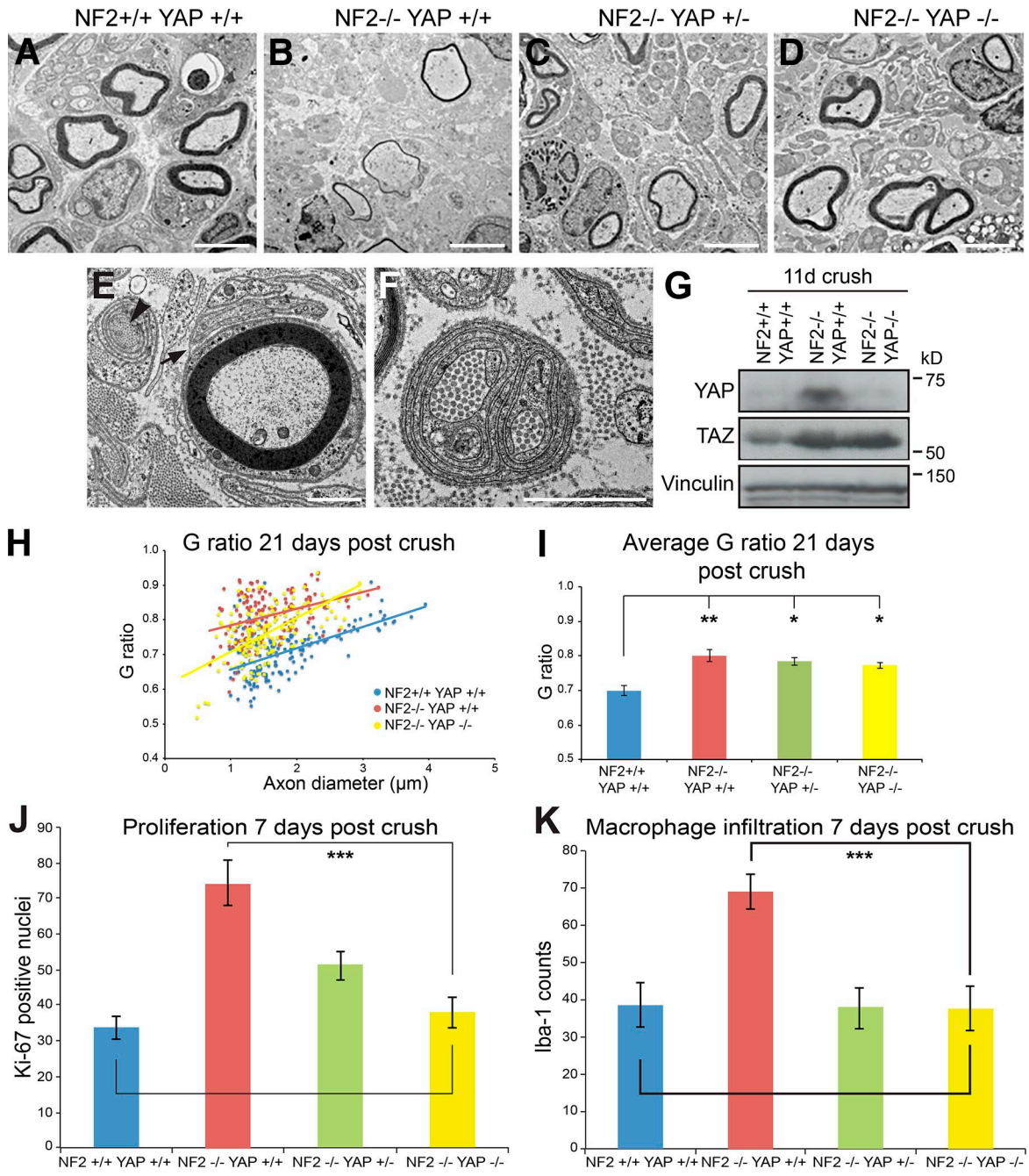

Figure 8. **Morphological analysis of nerves after injury and normalization of proliferation and macrophage infiltration in Merlin/YAP double-null nerves.** (A–D) Transmission EM images of the distal sciatic nerve at 21 d after crush injury showing remyelination of axons in NF2$^{-/-}$YAP$^{-/-}$ double-null nerves (D) compared with NF2$^{-/-}$YAP$^{+/+}$ Merlin-null animals (B). Mice with loss of one YAP allele (NF2$^{-/-}$YAP$^{+/-}$; C) have an intermediate phenotype. *n* = 3 mice for all genotypes. Bars, 5 µm. (E and F) Transmission EM pictures of Merlin/YAP double-null distal sciatic nerves at 21 d after injury showing SC processes and collagen wrapping by SCs within the nerve. The black arrow in E shows the continuous basal lamina of a myelinating SC with SC processes inside. The black arrowhead in E points to collagen wrapping, as also observed in F. Representative images from three biological replicates are shown. Bars, 1 µm. (G) Western blot 11 d after nerve crush injury showing loss of YAP induction in NF2$^{-/-}$YAP$^{-/-}$ distal sciatic nerves compared with NF2$^{-/-}$YAP$^{+/+}$ nerves. TAZ is up-regulated in both Merlin single-null and Merlin/YAP double-null distal sciatic nerves compared with control nerves after injury. Vinculin is used as a loading control. *n* = 3 pools; 1 pool = 3 nerves from three mice for each genotype. (H and I) Scatter plot graph (H) and mean (I) G ratio measurements 21 d after crush in Merlin-null and Merlin/YAP double-null distal sciatic nerves. (J and K) Graphs showing numbers of Ki67-positive proliferating cells (J) and numbers of Iba1-positive macrophages (K) in distal nerves of control, Merlin single-null, and Merlin/YAP double-null animals at 7 d after crush injury. Data are presented as means ± SEM. (H–K) *n* = 3 mice. (I–K) One-way analysis of variance with Bonferroni's multiple comparison test: *, P = 0.013 compared with NF2$^{-/-}$YAP$^{+/-}$; *, P = 0.021 compared with NF2$^{-/-}$ YAP$^{-/-}$ (F); **, P = 0.003 (I); ***, P ≤ 0.001 in the comparisons shown (J and K); P = 0.862 (J); P = 0.995 (K).

whether the effect of either MAPK is cJun dependent in vivo (Harrisingh et al., 2004; Fischer et al., 2008b; Napoli et al., 2012; Yang et al., 2012). It is possible that the increased activation of these MAPK pathways, together with increased macrophage numbers, may compensate for the reduced induction of cJun in regulating these events of Wallerian degeneration. Although the loss of axonal regeneration in Merlin-null nerves may be cJun dependent, both the increased SC proliferation and the inability

Published January 30, 2017

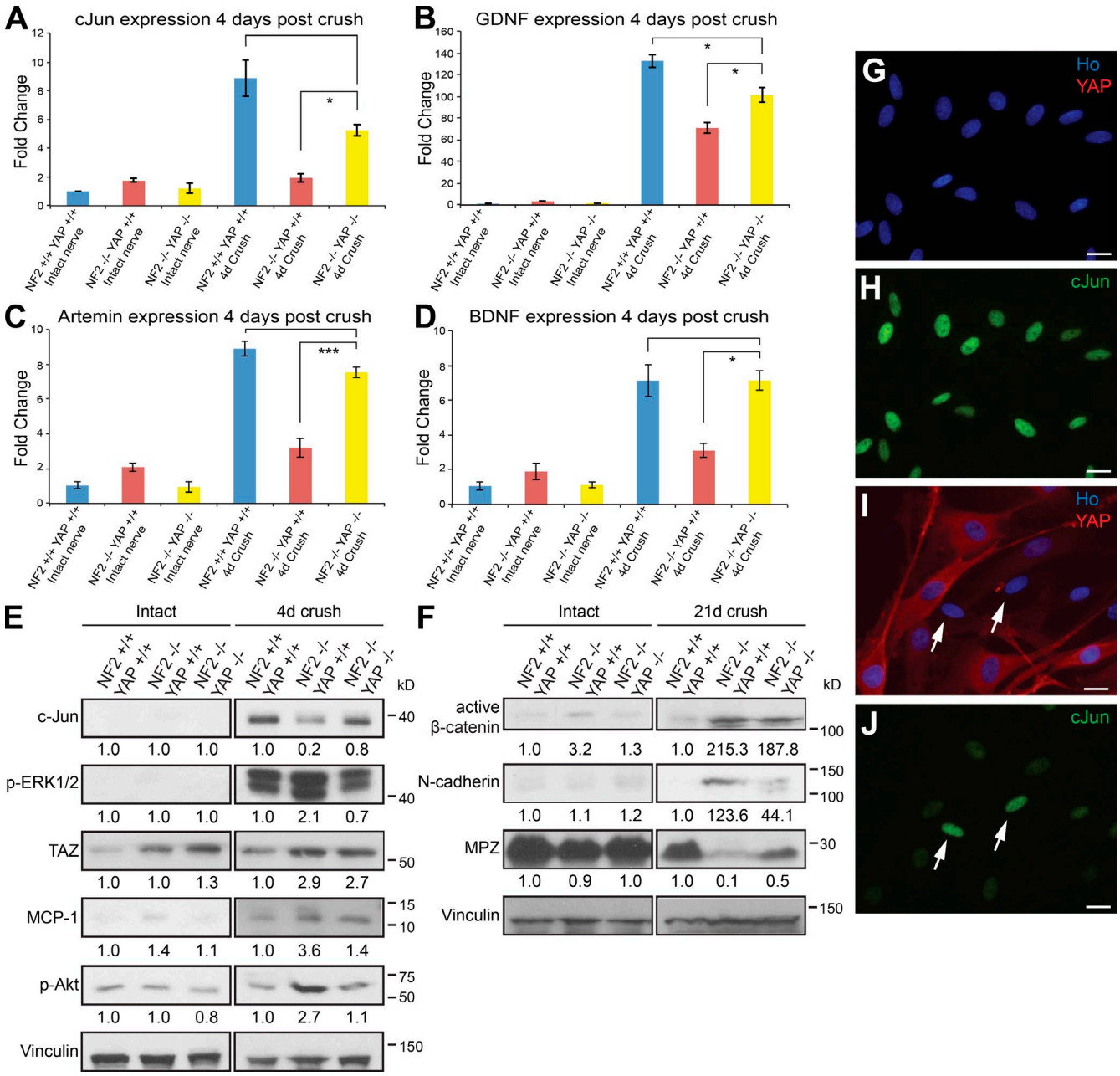

Figure 9. **Loss of YAP increases both cJun and neurotrophin expression in Merlin-null SCs after injury.** (A–D) Quantitative PCR measurements of cJun (A) and neurotrophin (B–D) expression 4 d after crush injury in control ($NF2^{+/+}YAP^{+/+}$), Merlin single-null ($NF2^{-/-}YAP^{+/+}$), and Merlin/YAP double-null ($NF2^{-/-}YAP^{-/-}$) animals. (A–D) One-way analysis of variance with Bonferroni's multiple comparison test: *, P = 0.048; P = 0.07 (A); *, P = 0.033 to $NF2^{-/-}YAP^{+/+}$; *, P = 0.028 to $NF2^{+/+}YAP^{+/+}$ (B); ***, $P \leq 0.001$; P = 0.218 (C); *, P = 0.016, P = 1 (D). Data are presented as means ± SEM. (E) Western blot showing cJun, p-ERK1/2, TAZ, MCP1, and p-Akt activation in control uninjured nerves and 4 d after crush injury in control, Merlin single-null, and Merlin/YAP double-null animals. Values represent normalized expression against the control. Vinculin is used as a loading control. (F) Western blot showing that loss of YAP in Merlin-null SCs increases myelin protein zero (MPZ) and reduces N-cadherin expression, but does not affect levels of activated β-catenin at 21 d after crush injury. (A–F) *n* = 3 pools; 1 pool = 3 nerves from three mice for each genotype. Values represent normalized expression against the control. Vinculin is used as a loading control. (G–J) YAP expression reduces levels of cJun in SCs. Immunolabeling of rat SCs expressing control LacZ (G and H) or $YAP^{Ser127Ala}$ (I and J) showing reduced levels of cJun protein in $YAP^{Ser127Ala}$-expressing cells (I and J). *n* = 3 experiments. Arrows in I and J indicate non–YAP-overexpressing SCs with unchanged levels of cJun protein. Bars, 20 µm.

to remyelinate the few regenerating axons after injury that we observed are not apparent in cJun-null animals (Arthur-Farraj et al., 2012). The increased severity of the regeneration defect seen in Merlin-null nerves indicates other targets of Merlin and YAP-dependent signaling in controlling these processes.

Other phenotypes observed in the Merlin-null nerves after injury, such as the wrapping of collagen fibers by SCs, are not observed in cJun-null nerves, but have been seen in mice with SC-specific loss of the phosphatase and tensin homologue (PTEN), with resulting increased PI3-kinase activity, and in mice expressing an activated form of Akt in SCs (Goebbels et al., 2010, 2012; Domènech-Estévez et al., 2016). Levels of p-Akt are increased in Merlin-null nerves after injury (Fig. 9 E), in keeping with the increased PI3-kinase/Akt signaling that has

Published January 30, 2017

been shown in human Merlin-null schwannoma cells in vitro (Ammoun et al., 2008). However, although this increased signaling through the PI3-kinase pathway may underlie the collagen wrapping by SCs and, perhaps, the increased deposition of basal lamina components (e.g., collagen type IV; Fig. 6 D) in Merlin-null nerves after injury (Domènech-Estévez et al., 2016), we clearly do not see the hypermyelination of axons seen in the PNS of these mouse PTEN mutants or Akt-overexpressing nerves either before or after injury in the Merlin-null nerves; indeed, we observed thinner remyelination of the few larger diameter axons that do regenerate after injury (Fig. 3, G and H). Loss of YAP in Merlin-null nerves appears to reduce levels of p-Akt after injury to those seen in control nerves (Fig. 9 E) and is associated with an improved remyelination of regenerating axons. One possible mechanism for this effect upon Akt activity is that YAP has been shown to down-regulate levels of PTEN protein by inducing the mRNA miR-29 that inhibits PTEN mRNA translation in cells (Tumaneng et al., 2012).

The cause of the increased collagen fibers seen in Merlin-null nerves after injury (Fig. 3, B, D, I, and J; and Fig. S2, I and J) is not clear, but recent data, using a mouse transgenic expressing a constitutively active Mek1 (Mek1DD), have shown that increased ERK1/2 activity in SCs is associated with increased collagen fiber deposition in the intact adult peripheral nerve (Ishii et al., 2016). Thus, it is possible that the increased ERK1/2 activity in Merlin-null nerves after injury (Fig. 6, C and D) drives the similar increase in collagen fibers within the nerve seen in our experiments.

Signaling through the Hippo pathway regulates multiple facets of cell behavior, including cell proliferation, cell fate, and ultimately tissue homeostasis and organ size (Yu et al., 2015). Regulation of the Hippo pathway by the Merlin protein has similarly been highly studied in the control of cell behavior in tumors with the loss of Merlin function and, in particular, with schwannomas and meningiomas of the nervous system (Asthagiri et al., 2009; Cooper and Giancotti, 2014; Li et al., 2014). Although the increased expression of YAP after injury is only seen in Merlin-null nerves, increased TAZ expression after injury is also seen in control nerves. Such a differential expression of YAP and TAZ has also been observed in the dorsal horn after nerve injury as well as in hepatocellular carcinoma tumors, highlighting potentially different roles for YAP and TAZ proteins in these situations (Hayashi et al., 2015; Xu et al., 2016). It remains to be determined whether there are distinct roles for these two Hippo pathway effectors in SCs in the events of nerve repair.

YAP-null nerves show no developmental defects and no defects in repair (Fig. S4, A–H), whereas TAZ-null nerves show some defects in axonal sorting (Poitelon et al., 2016; unpublished data). Recent work has shown that absence of both YAP and TAZ in SCs during development causes a severe peripheral neuropathy caused by defects in axonal sorting and that YAP/TAZ-dependent transcription regulates laminin receptors in SCs (Poitelon et al., 2016). The effects of TAZ loss alone in SCs upon PNS repair and whether loss of TAZ function will revert part or all of the phenotype of Merlin-null nerves after injury remain to be tested.

In conclusion, we have identified a completely novel function for the Merlin tumor suppressor in the control of SC reprogramming and PNS repair after injury. The finding that increased expression of YAP in Merlin-null nerves blocks the regenerative capacity of SCs to accomplish repair also demonstrates a new function for the Hippo/YAP pathway in this phenotype of Merlin-null nerves. These findings identify a potential novel mechanism for situations in which SCs may not be fully supportive and nerve repair may not be optimal, such as diabetic neuropathy, in the aging nerve (Painter et al., 2014), or situations that lead to longer term denervation of the distal nerve (Dahlin, 2013). Targeting of YAP-dependent signaling in such circumstances may, perhaps, offer an improvement in functional repair and outcome.

Materials and methods

Mice

All animal experiments conformed to UK Home Office regulations under the Animals (Scientific Procedures) Act of 1986. All breeding and surgical experiments have been approved by the Plymouth University Animal Welfare and Ethical Review Board. The P0-CRE mice (Feltri et al., 1999) were provided by L. Feltri and L. Wrabetz (University of New York at Buffalo, Buffalo, NY), and the conditional NF2 mice (Giovannini et al., 2000) were provided by M. Giovannini (University of California, Los Angeles, Los Angeles, CA). Animals with an SC-specific null of Merlin ($NF2^{fl/fl}$–$P0\text{-}CRE^{+}$) were made as previously described (Feltri et al., 1999; Giovannini et al., 2000; Doddrell et al., 2013); $NF2^{fl/fl}$–$P0\text{-}CRE^{-}$ littermates were used as controls. Merlin-null animals were crossed with YAP-conditional null ($YAP^{fl/fl}$) animals (Zhang et al., 2010) to generate Merlin-null animals with loss of either one or both YAP alleles in $P0\text{-}CRE^{+}$ animals; appropriate $P0\text{-}CRE^{-}$ animals were used as controls in these experiments. Genotyping of animals was performed as previously described (Feltri et al., 1999; Giovannini et al., 2000; Truett et al., 2000; Zhang et al., 2010). For developmental studies, approximately equal numbers of male and female mice were used with the appropriate sex and age-matched littermate controls.

Sciatic nerve injury, cut or crush, was performed in adult animals between 6 wk and 2 mo of age under isoflurane anesthesia as previously described (Dun and Parkinson, 2015), and distal sciatic or tibial nerve samples were taken at various time points after injury; contralateral uninjured nerves were used as controls. Once more, equal numbers of male and female mice were used with the appropriate sex and age-matched littermate controls for each experiment.

EM

Samples for low vacuum scanning or transmission EM were fixed in glutaraldehyde and embedded in resin blocks. For low vacuum scanning EM, sample block surfaces were polished and analyzed using a low vacuum scanning EM machine (6610; JEOL). For transmission EM, ultrathin sections were prepared, stained, and visualized using a microscope (1400; JEOL). Myelin thickness or G ratio (myelin thickness/myelin + axon thickness) measurements at stated time points were made from at least 200 myelinated fibers mid-sciatic nerve per animal. Measurements of axon and myelinated fiber (axon + myelin) diameter were made using ImageJ software (National Institutes of Health). Statistical significance difference was measured using the Mann-Whitney *U* test.

Mouse functional tests

The mouse SSI measurement (Baptista et al., 2007) was used to assess sensory–motor coordination in animals after sciatic nerve injury. Toe pinch tests were also used to assess recovery of sensory function (pressure sensitivity) as previously described (Arthur-Farraj et al., 2012). For single-frame motion analysis to evaluate recovery of locomotor function, mice were accustomed to beam walking 1 wk before surgery. Here, animals walk voluntarily from one end of a horizontal beam

Published January 30, 2017

(length, 1 m; width, 4 cm) toward the other end. For all mice, a rear view of one walking trial was captured with a video camera before surgery and at different time points after surgery. These video sequences were examined using VirtualDub 1.6.19 software. Selected frames, in which the animals could be seen in defined phases of the step cycle, were used for measurements of the foot–base angle, as described previously (Fey et al., 2010).

For rotarod testing, to measure motor function, 6–8-wk-old animals were placed on a rotating rod that accelerated from 2 to 30 rotations per minute over a time period of 250 s. The time taken for the animal to fall off (latency) was measured and recorded (Kuhn et al., 1995).

Electrophysiology

Investigation of sciatic nerve conduction characteristics was performed 5 wk after experimental nerve crush injury using previously described methods (Schulz et al., 2014b). Nerve conduction velocity tests in mice after crush injury were used to measure the efficiency of remyelination of the control and Merlin-null mouse nerves. The compound muscle action potential is a measure of the number of functional axons within the repairing nerve after injury and is an indicator of an impaired axonal regeneration when significantly reduced.

In brief, mice were anesthetized using isoflurane/O_2 inhalation. Hind limb fur was removed. A constant body temperature of 37°C was maintained by a heating plate and continuously measured by a rectal thermal probe. Needle electrodes were used to stimulate the sciatic nerve at both a proximal and distal stimulation site relative to the crush site. A ring electrode recorded the neuromuscular response from the gastrocnemius muscle.

Immunocytochemistry and Western blotting

Nerve samples were fixed in 4% paraformaldehyde/PBS overnight, cryoprotected in 30% sucrose/PBS overnight at 4°C, embedded in optimal cutting temperature compound, and frozen for cryosectioning. 10-µm sections for immunostaining were cut using a UV cryostat (CM1860; Leica Biosystems). For measurement of proliferation and macrophage numbers, control and mutant nerves were mounted within the same optimal cutting temperature block, and sections between 3 and 4 mm distal to the injury site, equidistant from the injury site for each genotype, were used for immunolabeling and counts. Sections were washed in PBS and blocked in either antibody-diluting solution (Parkinson et al., 2004) or 10% goat serum/PBS, supplemented with 0.2% Triton X-100 before addition of primary antibody. A two- or three-layer labeling system was used, using either a directly fluorophore-conjugated secondary antibody or a biotinylated secondary antibody followed by a streptavidin fluorophore conjugate. Samples were counterstained with Hoechst dye to reveal nuclei. Results presented for proliferation (Ki67-positive cells) and macrophage numbers (Iba1) are for the total number of positively stained cells within the nerve section. Three or more individual nerve sections of the same genotype were counted for each immunolabeling. Staining of teased nerve fibers with a fluorophore-conjugated phalloidin for assessment of internodal distance and Schmidt-Lanterman incisures was performed as described previously (Sharghi-Namini et al., 2006). Wholemount staining of nerve samples after injury was performed as described previously (Dun and Parkinson, 2015). Preparation, culture, and adenoviral infection of rat SCs was performed as described previously (Parkinson et al., 2004, 2008) using an adenovirus expressing $YAP^{Ser127Ala}$ or LacZ control (Shao et al., 2014). The control and YAP-expressing adenoviruses were gifts from S. Ikeda and J. Sadoshima (Rutgers University, New Brunswick, NJ). For Western blotting, samples from control and injured nerves were frozen in liquid nitrogen. Nerves from three mice were grouped together for each genotype and time point to create a pooled sample. Sample extraction, gel electrophoresis, and analysis were all as previously described (Parkinson et al., 2003, 2004). Equal loading of samples was ensured by both protein estimation and use of colloidal gold to stain membranes after transfer (Parkinson et al., 2003, 2004).

Primary antibodies

The following primary antibodies were used for immunofluorescence staining at the indicated dilutions: neurofilament (NF200) heavy 200 kD (1:500; ab4680; Abcam), cJun (1:200; 9165S; Cell Signaling Technology), Iba1 (1:300; 019–19741; Wako Pure Chemical Industries), F4/80 (1:300; ab16911; Abcam), and Ki67 (1:200; ab15580; Abcam).

The following primary antibodies were used for Western blotting: myelin protein zero (1:1,000; SAB2500665; Sigma-Aldrich), MBP (1:2,000; sc-13912; Santa Cruz Biotechnology, Inc.), Krox20 (1:500; PRB-236P-100; Covance), β-tubulin (1:2,000; sc-134229; Santa Cruz Biotechnology, Inc.), cJun (1:1,000; 9165; Cell Signaling Technology), p-cJun (1:500; 9261; Cell Signaling Technology), p-Erk1/2 (1:2,000; 9101; Cell Signaling Technology), p-p38 (1:500; 4631; Cell Signaling Technology), YAP/TAZ (1:1,000; 8418; Cell Signaling Technology), TAZ (1:1,000; 4883; Cell Signaling Technology), YAP (1:1,000; 14074; Cell Signaling Technology), connective tissue growth factor (1:1,000; ab6992; Abcam), collagen IV (1:1,000; ab6586; Abcam), MCP1 (1:500; 500-P113; PeproTech), active β-catenin (1:1,000; 05–665; EMD Millipore), N-cadherin (1:1,000; ab76057; Abcam), E-cadherin (1:1,000; PharMingen Clone 36 610181; BD), p-Akt (1:2,000; 4060; Cell Signaling Technology), and vinculin (1:1,000; 4650; Cell Signaling Technology).

Histology and immunohistochemistry

For hematoxylin and eosin (H&E) staining, mice were sacrificed, and sciatic nerves were dissected and postfixed in 10% formalin for 24 h at 4°C. Sciatic nerves were cut into three segments: proximal, injury site, and distal. Samples were then dehydrated in ethanol followed by xylene and embedded in paraffin. Sciatic nerve segments were cut transversely into 4-µm sections using a microstat (Leica Biosystems). Sciatic nerve sections were deparaffinized with xylene and rehydrated through a graded ethanol series to water before H&E staining (Sigma-Aldrich). For MBP staining, the sections were subjected to pretreatment with EDTA, pH 9.0, for 30 min. Sections were then incubated overnight with the primary antibody goat anti-MBP (1:1,000; sc-13912; Santa Cruz Biotechnology, Inc.). Immunostaining was visualized by an avidin–biotin complex method, followed by light counterstaining with hematoxylin. For the axonal visualization, 10-µm sections were cut and stained according to Palmgren's silver stain method. Staining with Masson's trichrome stain was performed as per the manufacturer's protocol (Abcam).

Quantitative PCR analysis

Distal nerve stumps to the crush site were collected at 4 d after crush injury in mice and frozen in liquid nitrogen. Nerves from three mice were grouped together for each genotype and time point to create a pooled sample. Samples were crushed and homogenized on dry ice and then lysed in QIAzol lysis reagent (QIAGEN), and RNA was purified using the miRNeasy mini kit (QIAGEN). After RNA purification, RNA was reverse transcribed using the High Capacity RNA-to-cDNA kit (Applied Biosystems). Quantitative PCR was then performed using the Power SYBR Green PCR Master Mix (Applied Biosystems). Analysis was performed with three technical replicates per sample. Relative expression values for each gene of interest were obtained by normalizing to Rpl13 (Pratt-Hyatt et al., 2013), and fold changes were determined with the Livak method. Primer sequences used for quantitative PCR have been published previously (Arthur-Farraj et al., 2012).

Published January 30, 2017

Statistical analysis

Statistical analysis was performed using SPSS (IBM) or Excel (Microsoft). The two-sided two-sample Student's *t* test or the one-way analysis of variance with Bonferroni's multiple comparison test (because of the power it has for small sample sizes) was used depending on the number of the samples. Statistical significance has been reported as *, $P \leq 0.05$; **, $P \leq 0.01$; and ***, $P \leq 0.001$. Because of the small sample sizes ($n < 5$ for most statistical comparisons), assumptions of how well normality and equal variances fit the data could not be reliably assessed. Sample size was not predetermined by statistical methods and randomization was not applied. The investigators were not blinded to group allocation during the experiments because the mutant nerves displayed obvious behavioral and morphological characteristics after nerve injury. No samples or data were excluded from the analysis. Biological replicates were used in all the experiments, and these are represented in all the data plots. The *n* number of each experiment has been reported in all the figures. In brief, in most cases *n* is defined as the number of mice from the same genotype and same experiment. Samples for Western blotting and quantitative PCR were prepared by grouping nerves from three mice together for each genotype and time point to create a pooled sample. We have used pooled biological replicates for the repetition of these experiments. All data are represented in the figures as mean values ± SEM.

Online supplemental material

Fig. S1 describes the G ratio of Merlin-null nerves at an additional time point, P21, and the nuclei counts in longitudinal sections of adult Merlin-null nerves. Fig. S2 shows the regeneration, remyelination, collagen, and tissue histology of Merlin-null nerves at 8 mo after injury. Fig. S3 presents the sensory recovery, as measured by toe pinch, of Merlin-null animals after sciatic nerve crush injury. Fig. S4 characterizes the YAP-null animals before and after injury. Fig. S5 characterizes the Merlin/YAP double-null animals before sciatic nerve crush injury.

Acknowledgments

We are grateful for excellent technical support from Dr. R. Moate, Mr. P. Bond, and Mr. G. Harper in the Plymouth University EM Centre for help with EM processing and imaging. We thank Professors L. Feltri and L. Wrabetz for providing the P0-CRE mice and Professor M. Giovannini for the conditional NF2 mice. We are grateful to Professors R. Mirsky and K.R. Jessen for comments on the manuscript. We thank Dr. S. Ikeda and Professor J. Sadoshima for the LacZ and YAP-expressing adenoviruses, Dr. W.A. Woldie for help with quantitative PCR, and Mr. W. Woznica for excellent technical support with animal husbandry.

This work was supported by grants from the UK Medical Research Council (MR/J012785/1) and the Northcott Devon Medical Foundation (TB/MG/NO5002) to D.B. Parkinson.

The authors declare no competing financial interests.

Author contributions: T. Mindos, X.-p. Dun, K. North, R.D.S. Doddrell, S.L. Roberts, A. Schulz, J. Russel, G. Mortimer, and D.B. Parkinson designed experiments and analyzed data. B. Gray, P. Edwards, and A. Schulz performed experiments and analyzed data. N. Zhang and D. Pan provided transgenic mice and experimental guidance. T. Mindos, H. Morrison, and D.B. Parkinson wrote and edited the manuscript.

Submitted: 10 June 2016
Revised: 23 October 2016
Accepted: 27 December 2016

References

Ammoun, S., C. Flaiz, N. Ristic, J. Schuldt, and C.O. Hanemann. 2008. Dissecting and targeting the growth factor-dependent and growth factor-independent extracellular signal-regulated kinase pathway in human schwannoma. *Cancer Res.* 68:5236–5245. http://dx.doi.org/10.1158/0008-5472.CAN-07-5849

Arthur-Farraj, P.J., M. Latouche, D.K. Wilton, S. Quintes, E. Chabrol, A. Banerjee, A. Woodhoo, B. Jenkins, M. Rahman, M. Turmaine, et al. 2012. c-Jun reprograms Schwann cells of injured nerves to generate a repair cell essential for regeneration. *Neuron.* 75:633–647. http://dx.doi.org/10.1016/j.neuron.2012.06.021

Asthagiri, A.R., D.M. Parry, J.A. Butman, H.J. Kim, E.T. Tsilou, Z. Zhuang, and R.R. Lonser. 2009. Neurofibromatosis type 2. *Lancet.* 373:1974–1986. http://dx.doi.org/10.1016/S0140-6736(09)60259-2

Baptista, A.F., J.R. Gomes, J.T. Oliveira, S.M. Santos, M.A. Vannier-Santos, and A.M. Martinez. 2007. A new approach to assess function after sciatic nerve lesion in the mouse—adaptation of the sciatic static index. *J. Neurosci. Methods.* 161:259–264. http://dx.doi.org/10.1016/j.jneumeth.2006.11.016

Cooper, J., and F.G. Giancotti. 2014. Molecular insights into NF2/Merlin tumor suppressor function. *FEBS Lett.* 588:2743–2752. http://dx.doi.org/10.1016/j.febslet.2014.04.001

Crawford, A.T., D. Desai, P. Gokina, S. Basak, and H.A. Kim. 2008. E-cadherin expression in postnatal Schwann cells is regulated by the cAMP-dependent protein kinase a pathway. *Glia.* 56:1637–1647. http://dx.doi.org/10.1002/glia.20716

Dahlin, L.B. 2013. The role of timing in nerve reconstruction. *Int. Rev. Neurobiol.* 109:151–164. http://dx.doi.org/10.1016/B978-0-12-420045-6.00007-9

Denisenko, N., C. Cifuentes-Diaz, T. Irinopoulou, M. Carnaud, E. Benoit, M. Niwa-Kawakita, F. Chareyre, M. Giovannini, J.A. Girault, and L. Goutebroze. 2008. Tumor suppressor schwannomin/Merlin is critical for the organization of Schwann cell contacts in peripheral nerves. *J. Neurosci.* 28:10472–10481. http://dx.doi.org/10.1523/JNEUROSCI.2537-08.2008

de Vries, M., I. Briaire-de Bruijn, M.J. Malessy, S.F. de Bruïne, A.G. van der Mey, and P.C. Hogendoorn. 2013. Tumor-associated macrophages are related to volumetric growth of vestibular schwannomas. *Otol. Neurotol.* 34:347–352. http://dx.doi.org/10.1097/MAO.0b013e31827c9fbf

Doddrell, R.D., X.P. Dun, A. Shivane, M.L. Feltri, L. Wrabetz, M. Wegner, E. Sock, C.O. Hanemann, and D.B. Parkinson. 2013. Loss of SOX10 function contributes to the phenotype of human Merlin-null schwannoma cells. *Brain.* 136:549–563. http://dx.doi.org/10.1093/brain/aws353

Domènech-Estévez, E., H. Baloui, X. Meng, Y. Zhang, K. Deinhardt, J.L. Dupree, S. Einheber, R. Chrast, and J.L. Salzer. 2016. Akt regulates axon wrapping and myelin sheath thickness in the PNS. *J. Neurosci.* 36:4506–4521. http://dx.doi.org/10.1523/JNEUROSCI.3521-15.2016

Dun, X.P., and D.B. Parkinson. 2015. Visualizing peripheral nerve regeneration by whole mount staining. *PLoS One.* 10. http://dx.doi.org/10.1371/journal.pone.0119168

Feltri, M.L., M. D'Antonio, S. Previtali, M. Fasolini, A. Messing, and L. Wrabetz. 1999. *P_0-Cre* transgenic mice for inactivation of adhesion molecules in Schwann cells. *Ann. N. Y. Acad. Sci.* 883:116–123. http://dx.doi.org/10.1111/j.1749-6632.1999.tb08574.x

Fey, A., M. Schachner, and A. Irintchev. 2010. A novel motion analysis approach reveals late recovery in C57BL/6 mice and deficits in NCAM-deficient mice after sciatic nerve crush. *J. Neurotrauma.* 27:815–828. http://dx.doi.org/10.1089/neu.2009.1217

Fischer, S., C. Kleinschnitz, M. Müller, I. Kobsar, C.W. Ip, B. Rollins, and R. Martini. 2008a. Monocyte chemoattractant protein-1 is a pathogenic component in a model for a hereditary peripheral neuropathy. *Mol. Cell. Neurosci.* 37:359–366. http://dx.doi.org/10.1016/j.mcn.2007.10.012

Fischer, S., A. Weishaupt, J. Troppmair, and R. Martini. 2008b. Increase of MCP-1 (CCL2) in myelin mutant Schwann cells is mediated by MEK-ERK signaling pathway. *Glia.* 56:836–843. http://dx.doi.org/10.1002/glia.20657

Fontana, X., M. Hristova, C. Da Costa, S. Patodia, L. Thei, M. Makwana, B. Spencer-Dene, M. Latouche, R. Mirsky, K.R. Jessen, et al. 2012. c-Jun in Schwann cells promotes axonal regeneration and motoneuron survival via paracrine signaling. *J. Cell Biol.* 198:127–141. http://dx.doi.org/10.1083/jcb.201205025

Gehlhausen, J.R., S.J. Park, A.E. Hickox, M. Shew, K. Staser, S.D. Rhodes, K. Menon, J.D. Lajiness, M. Mwanthi, X. Yang, et al. 2015. A murine model of neurofibromatosis type 2 that accurately phenocopies human schwannoma formation. *Hum. Mol. Genet.* 24:1–8. http://dx.doi.org/10.1093/hmg/ddu414

Giovannini, M., E. Robanus-Maandag, M. van der Valk, M. Niwa-Kawakita, V. Abramowski, L. Goutebroze, J.M. Woodruff, A. Berns, and G. Thomas.

2000. Conditional biallelic Nf2 mutation in the mouse promotes manifestations of human neurofibromatosis type 2. *Genes Dev.* 14:1617–1630.

Goebbels, S., J.H. Oltrogge, R. Kemper, I. Heilmann, I. Bormuth, S. Wolfer, S.P. Wichert, W. Möbius, X. Liu, C. Lappe-Siefke, et al. 2010. Elevated phosphatidylinositol 3,4,5-trisphosphate in glia triggers cell-autonomous membrane wrapping and myelination. *J. Neurosci.* 30:8953–8964. http://dx.doi.org/10.1523/JNEUROSCI.0219-10.2010

Goebbels, S., J.H. Oltrogge, S. Wolfer, G.L. Wieser, T. Nientiedt, A. Pieper, T. Ruhwedel, M. Groszer, M.W. Sereda, and K.A. Nave. 2012. Genetic disruption of *Pten* in a novel mouse model of tomaculous neuropathy. *EMBO Mol. Med.* 4:486–499. http://dx.doi.org/10.1002/emmm.201200227

Hanemann, C.O. 2008. Magic but treatable? Tumours due to loss of Merlin. *Brain.* 131:606–615. http://dx.doi.org/10.1093/brain/awm249

Harrisingh, M.C., E. Perez-Nadales, D.B. Parkinson, D.S. Malcolm, A.W. Mudge, and A.C. Lloyd. 2004. The Ras/Raf/ERK signalling pathway drives Schwann cell dedifferentiation. *EMBO J.* 23:3061–3071. http://dx.doi.org/10.1038/sj.emboj.7600309

Hayashi, H., T. Higashi, N. Yokoyama, T. Kaida, K. Sakamoto, Y. Fukushima, T. Ishimoto, H. Kuroki, H. Nitta, D. Hashimoto, et al. 2015. An imbalance in TAZ and YAP expression in hepatocellular carcinoma confers cancer stem cell-like behaviors contributing to disease progression. *Cancer Res.* 75:4985–4997. http://dx.doi.org/10.1158/0008-5472.CAN-15-0291

Hilton, D.A., and C.O. Hanemann. 2014. Schwannomas and their pathogenesis. *Brain Pathol.* 24:205–220. http://dx.doi.org/10.1111/bpa.12125

Ishii, A., M. Furusho, J.L. Dupree, and R. Bansal. 2016. Strength of ERK1/2 MAPK activation determines its effect on myelin and axonal integrity in the adult CNS. *J. Neurosci.* 36:6471–6487. http://dx.doi.org/10.1523/JNEUROSCI.0299-16.2016

Jessen, K.R., and R. Mirsky. 2016. The repair Schwann cell and its function in regenerating nerves. *J. Physiol.* 594:3521–3531. http://dx.doi.org/10.1113/JP270874

Jessen, K.R., R. Mirsky, and P. Arthur-Farraj. 2015. The role of cell plasticity in tissue repair: adaptive cellular reprogramming. *Dev. Cell.* 34:613–620. http://dx.doi.org/10.1016/j.devcel.2015.09.005

Kang, H., and J.W. Lichtman. 2013. Motor axon regeneration and muscle reinnervation in young adult and aged animals. *J. Neurosci.* 33:19480–19491. http://dx.doi.org/10.1523/JNEUROSCI.4067-13.2013

Kim, H.A., T. Mindos, and D.B. Parkinson. 2013. Plastic fantastic: Schwann cells and repair of the peripheral nervous system. *Stem Cells Transl. Med.* 2:553–557. http://dx.doi.org/10.5966/sctm.2013-0011

Kuhn, P.L., E. Petroulakis, G.A. Zazanis, and R.D. McKinnon. 1995. Motor function analysis of myelin mutant mice using a rotarod. *Int. J. Dev. Neurosci.* 13:715–722. http://dx.doi.org/10.1016/0736-5748(96)81215-9

Li, W., J. Cooper, L. Zhou, C. Yang, H. Erdjument-Bromage, D. Zagzag, M. Snuderl, M. Ladanyi, C.O. Hanemann, P. Zhou, et al. 2014. Merlin/NF2 loss-driven tumorigenesis linked to $CRL4^{DCAF1}$-mediated inhibition of the Hippo pathway kinases Lats1 and 2 in the nucleus. *Cancer Cell.* 26:48–60. http://dx.doi.org/10.1016/j.ccr.2014.05.001

Myers, R.R., Y. Sekiguchi, S. Kikuchi, B. Scott, S. Medicherla, A. Protter, and W.M. Campana. 2003. Inhibition of p38 MAP kinase activity enhances axonal regeneration. *Exp. Neurol.* 184:606–614. http://dx.doi.org/10.1016/S0014-4886(03)00297-8

Napoli, I., L.A. Noon, S. Ribeiro, A.P. Kerai, S. Parrinello, L.H. Rosenberg, M.J. Collins, M.C. Harrisingh, I.J. White, A. Woodhoo, and A.C. Lloyd. 2012. A central role for the ERK-signaling pathway in controlling Schwann cell plasticity and peripheral nerve regeneration in vivo. *Neuron.* 73:729–742. http://dx.doi.org/10.1016/j.neuron.2011.11.031

Painter, M.W., A. Brosius Lutz, Y.C. Cheng, A. Latremoliere, K. Duong, C.M. Miller, S. Posada, E.J. Cobos, A.X. Zhang, A.J. Wagers, et al. 2014. Diminished Schwann cell repair responses underlie age-associated impaired axonal regeneration. *Neuron.* 83:331–343. http://dx.doi.org/10.1016/j.neuron.2014.06.016

Parkinson, D.B., S. Dickinson, A. Bhaskaran, M.T. Kinsella, P.J. Brophy, D.L. Sherman, S. Sharghi-Namini, M.B. Duran Alonso, R. Mirsky, and K.R. Jessen. 2003. Regulation of the myelin gene periaxin provides evidence for Krox-20-independent myelin-related signalling in Schwann cells. *Mol. Cell. Neurosci.* 23:13–27. http://dx.doi.org/10.1016/S1044-7431(03)00024-1

Parkinson, D.B., A. Bhaskaran, A. Droggiti, S. Dickinson, M. D'Antonio, R. Mirsky, and K.R. Jessen. 2004. Krox-20 inhibits Jun-NH_2-terminal kinase/c-Jun to control Schwann cell proliferation and death. *J. Cell Biol.* 164:385–394. http://dx.doi.org/10.1083/jcb.200307132

Parkinson, D.B., A. Bhaskaran, P. Arthur-Farraj, L.A. Noon, A. Woodhoo, A.C. Lloyd, M.L. Feltri, L. Wrabetz, A. Behrens, R. Mirsky, and K.R. Jessen. 2008. c-Jun is a negative regulator of myelination. *J. Cell Biol.* 181:625–637. http://dx.doi.org/10.1083/jcb.200803013

Poitelon, Y., C. Lopez-Anido, K. Catignas, C. Berti, M. Palmisano, C. Williamson, D. Ameroso, K. Abiko, Y. Hwang, A. Gregorieff, et al. 2016. YAP and TAZ control peripheral myelination and the expression of laminin receptors in Schwann cells. *Nat. Neurosci.* 19:879–887. http://dx.doi.org/10.1038/nn.4316

Pratt-Hyatt, M., A.J. Lickteig, and C.D. Klaassen. 2013. Tissue distribution, ontogeny, and chemical induction of aldo-keto reductases in mice. *Drug Metab. Dispos.* 41:1480–1487. http://dx.doi.org/10.1124/dmd.113.051904

Schulz, A., S.L. Baader, M. Niwa-Kawakita, M.J. Jung, R. Bauer, C. Garcia, A. Zoch, S. Schacke, C. Hagel, V.F. Mautner, et al. 2013. Merlin isoform 2 in neurofibromatosis type 2-associated polyneuropathy. *Nat. Neurosci.* 16:426–433. http://dx.doi.org/10.1038/nn.3348

Schulz, A., A. Kyselyova, S.L. Baader, M.J. Jung, A. Zoch, V.F. Mautner, C. Hagel, and H. Morrison. 2014a. Neuronal Merlin influences ERBB2 receptor expression on Schwann cells through neuregulin 1 type III signalling. *Brain.* 137:420–432. http://dx.doi.org/10.1093/brain/awt327

Schulz, A., C. Walther, H. Morrison, and R. Bauer. 2014b. *In vivo* electrophysiological measurements on mouse sciatic nerves. *J. Vis. Exp.* 86. http://dx.doi.org/10.3791/51181

Schulz, A., R. Büttner, C. Hagel, S.L. Baader, L. Kluwe, J. Salamon, V.F. Mautner, T. Mindos, D.B. Parkinson, J.R. Gehlhausen, et al. 2016. The importance of nerve microenvironment for schwannoma development. *Acta Neuropathol.* 132:289–307. http://dx.doi.org/10.1007/s00401-016-1583-8

Shao, D., P. Zhai, D.P. Del Re, S. Sciarretta, N. Yabuta, H. Nojima, D.S. Lim, D. Pan, and J. Sadoshima. 2014. A functional interaction between Hippo-YAP signalling and FoxO1 mediates the oxidative stress response. *Nat. Commun.* 5. http://dx.doi.org/10.1038/ncomms4315

Sharghi-Namini, S., M. Turmaine, C. Meier, V. Sahni, F. Umehara, K.R. Jessen, and R. Mirsky. 2006. The structural and functional integrity of peripheral nerves depends on the glial-derived signal desert hedgehog. *J. Neurosci.* 26:6364–6376. http://dx.doi.org/10.1523/JNEUROSCI.0157-06.2006

Shimomura, T., N. Miyamura, S. Hata, R. Miura, J. Hirayama, and H. Nishina. 2014. The PDZ-binding motif of Yes-associated protein is required for its co-activation of TEAD-mediated CTGF transcription and oncogenic cell transforming activity. *Biochem. Biophys. Res. Commun.* 443:917–923. http://dx.doi.org/10.1016/j.bbrc.2013.12.100

Tofaris, G.K., P.H. Patterson, K.R. Jessen, and R. Mirsky. 2002. Denervated Schwann cells attract macrophages by secretion of leukemia inhibitory factor (LIF) and monocyte chemoattractant protein-1 in a process regulated by interleukin-6 and LIF. *J. Neurosci.* 22:6696–6703.

Truett, G.E., P. Heeger, R.L. Mynatt, A.A. Truett, J.A. Walker, and M.L. Warman. 2000. Preparation of PCR-quality mouse genomic DNA with hot sodium hydroxide and tris (HotSHOT). *Biotechniques.* 29:52–54.

Tumaneng, K., K. Schlegelmilch, R.C. Russell, D. Yimlamai, H. Basnet, N. Mahadevan, J. Fitamant, N. Bardeesy, F.D. Camargo, and K.L. Guan. 2012. YAP mediates crosstalk between the Hippo and PI(3)K–TOR pathways by suppressing PTEN via miR-29. *Nat. Cell Biol.* 14:1322–1329. http://dx.doi.org/10.1038/ncb2615

Xu, N., M.Z. Wu, X.T. Deng, P.C. Ma, Z.H. Li, L. Liang, M.F. Xia, D. Cui, D.D. He, Y. Zong, et al. 2016. Inhibition of YAP/TAZ activity in spinal cord suppresses neuropathic pain. *J. Neurosci.* 36:10128–10140. http://dx.doi.org/10.1523/JNEUROSCI.0800-16.2016

Yang, D.P., D.P. Zhang, K.S. Mak, D.E. Bonder, S.L. Pomeroy, and H.A. Kim. 2008. Schwann cell proliferation during Wallerian degeneration is not necessary for regeneration and remyelination of the peripheral nerves: axon-dependent removal of newly generated Schwann cells by apoptosis. *Mol. Cell. Neurosci.* 38:80–88. http://dx.doi.org/10.1016/j.mcn.2008.01.017

Yang, D.P., J. Kim, N. Syed, Y.J. Tung, A. Bhaskaran, T. Mindos, R. Mirsky, K.R. Jessen, P. Maurel, D.B. Parkinson, and H.A. Kim. 2012. p38 MAPK activation promotes denervated Schwann cell phenotype and functions as a negative regulator of Schwann cell differentiation and myelination. *J. Neurosci.* 32:7158–7168. http://dx.doi.org/10.1523/JNEUROSCI.5812-11.2012

Yu, F.X., B. Zhao, and K.L. Guan. 2015. Hippo pathway in organ size control, tissue homeostasis, and cancer. *Cell.* 163:811–828. http://dx.doi.org/10.1016/j.cell.2015.10.044

Zhang, N., H. Bai, K.K. David, J. Dong, Y. Zheng, J. Cai, M. Giovannini, P. Liu, R.A. Anders, and D. Pan. 2010. The Merlin/NF2 tumor suppressor functions through the YAP oncoprotein to regulate tissue homeostasis in mammals. *Dev. Cell.* 19:27–38. http://dx.doi.org/10.1016/j.devcel.2010.06.015

Zhao, B., L. Li, Q. Lei, and K.L. Guan. 2010. The Hippo-YAP pathway in organ size control and tumorigenesis: an updated version. *Genes Dev.* 24:862–874. http://dx.doi.org/10.1101/gad.1909210

Mindos et al., https://doi.org/10.1083/jcb.201606052

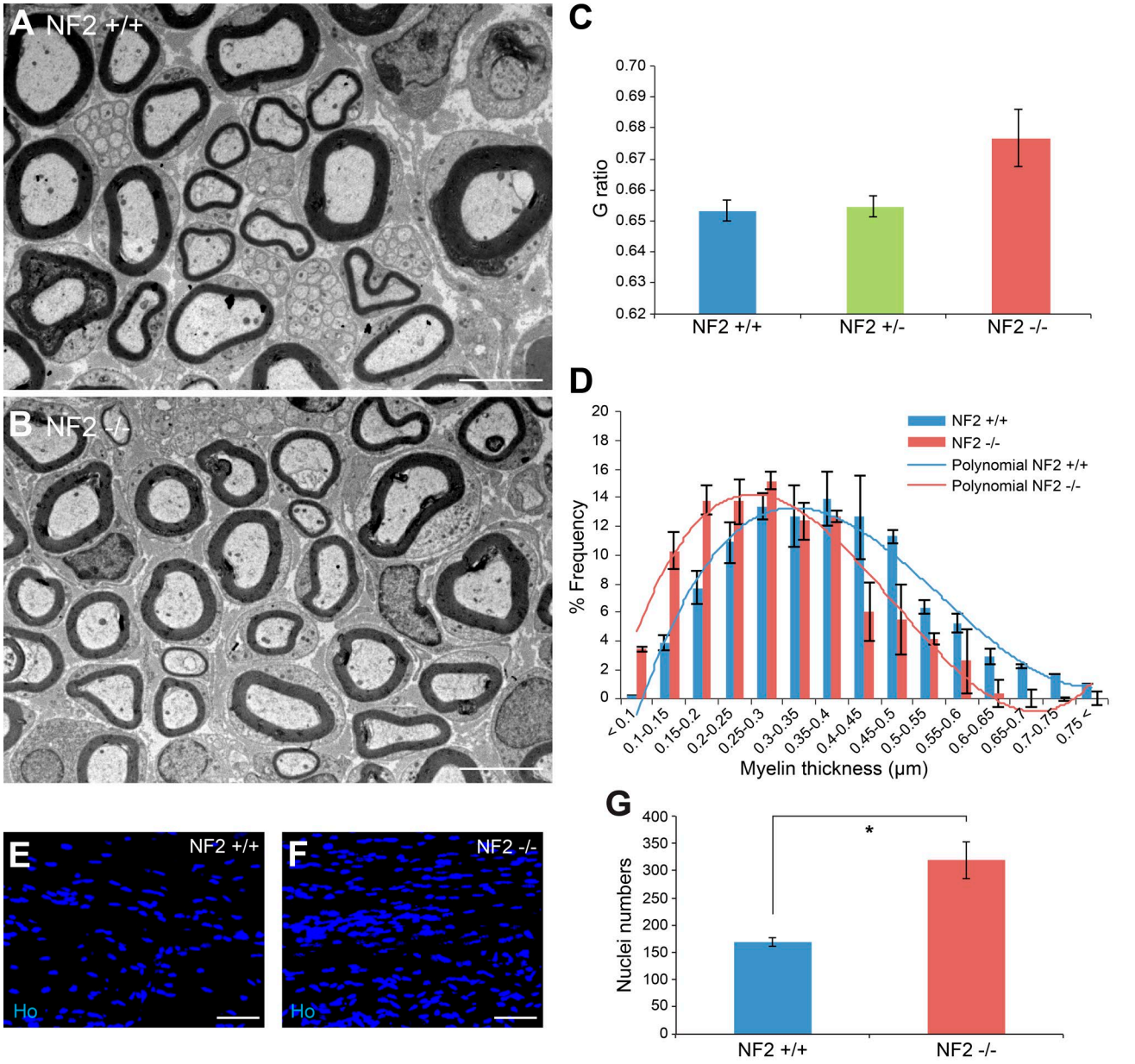

Figure S1. **Myelination and nuclei counts in nerves with SC-specific loss of Merlin.** (A and B) Transmission EM pictures of P21 control ($NF2^{+/+}$) and Merlin-null ($NF2^{-/-}$) nerves. Bars, 5 µm. (C) G ratio measurements of sciatic nerves from P21 control, Merlin heterozygous ($NF2^{+/-}$), and Merlin-null nerves. (D) Graph showing distribution of myelin thickness in P6 control and Merlin-null nerves. (A–D) $n = 3$ mice. (E–G) Hoechst-stained nuclei (E and F) and quantification (G) of longitudinal cryostat sections from adult intact sciatic nerves showing an increase in cell number in Merlin-null (F) nerves compared with control (E). Data are presented as means ± SEM. (E and F) $NF2^{+/+}$, $n = 3$ (E); $NF2^{-/-}$, $n = 5$ (F). Bars, 25 µm. (G) Two-sided two-sample Student's *t* test: *, P = 0.017.

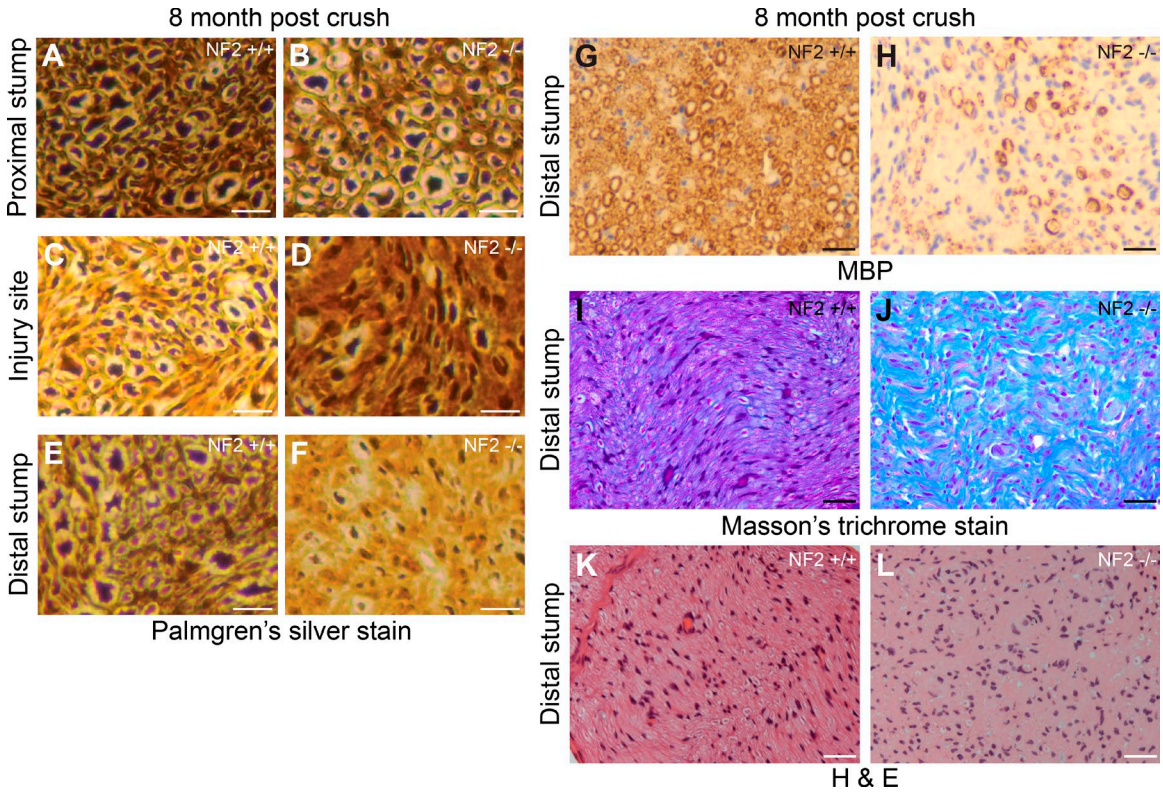

Figure S2. **Axonal regeneration, remyelination, and histology of control and Merlin-null nerves 8 mo after injury.** (A–F) Palmgren's silver stain showing axonal regeneration in control ($NF2^{+/+}$) and Merlin-null ($NF2^{-/-}$) nerves at 8 mo after crush injury. Sections of proximal nerve (A and B), injury site (C and D), and distal nerve (E and F) were stained to visualize axons with Palmgren's silver stain. Bars, 10 µm. (G and H) MBP immunolabeling of sections of the control (G) and Merlin-null (H) distal sciatic nerve showing low levels of MBP-positive remyelinated fibers in Merlin-null nerves at 8 mo after injury. (A–H) *n* = 6 mice. Bars, 50 µm. (I and J) Masson's trichrome stain showing collagen deposition (blue) in control (I) and Merlin-null (J) distal nerves at 8 mo after injury. Masson's trichrome staining colors the connective tissue blue and the cytoplasm red. Bars, 50 µm. (K and L) Hematoxylin and eosin (H&E) staining of control (K) and Merlin-null (L) distal nerves at 8 mo after injury. *n* = 6 mice. Bars, 50 µm.

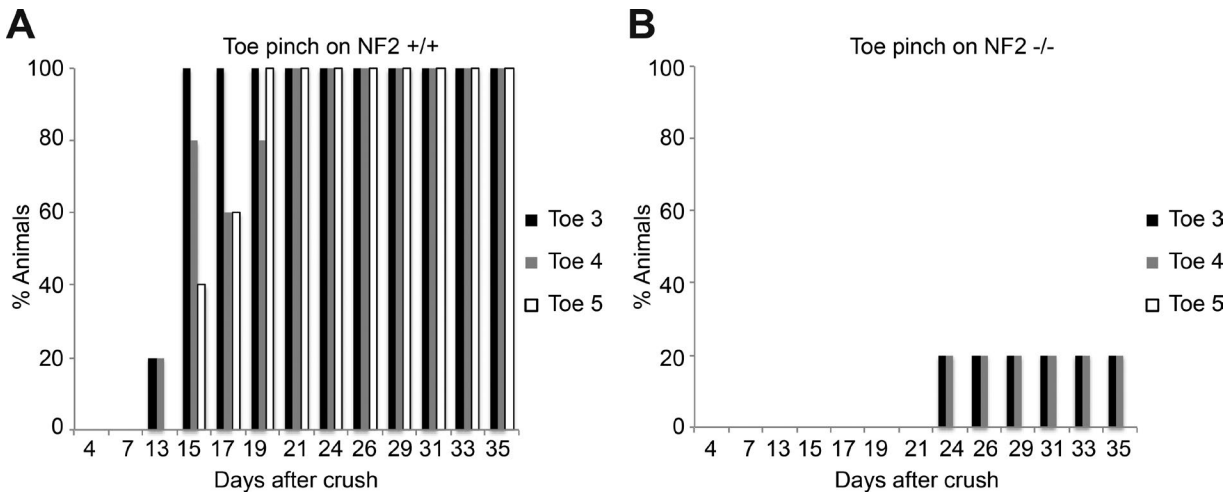

Figure S3. **Functional sensory testing of control and Merlin-null animals after crush injury.** (A and B) Graph of toe pinch data to measure sensory recovery at time points up to 35 d after injury for control ($NF2^{+/+}$) and Merlin-null ($NF2^{-/-}$) animals. Data are presented as means ± SEM. *n* = 5 mice.

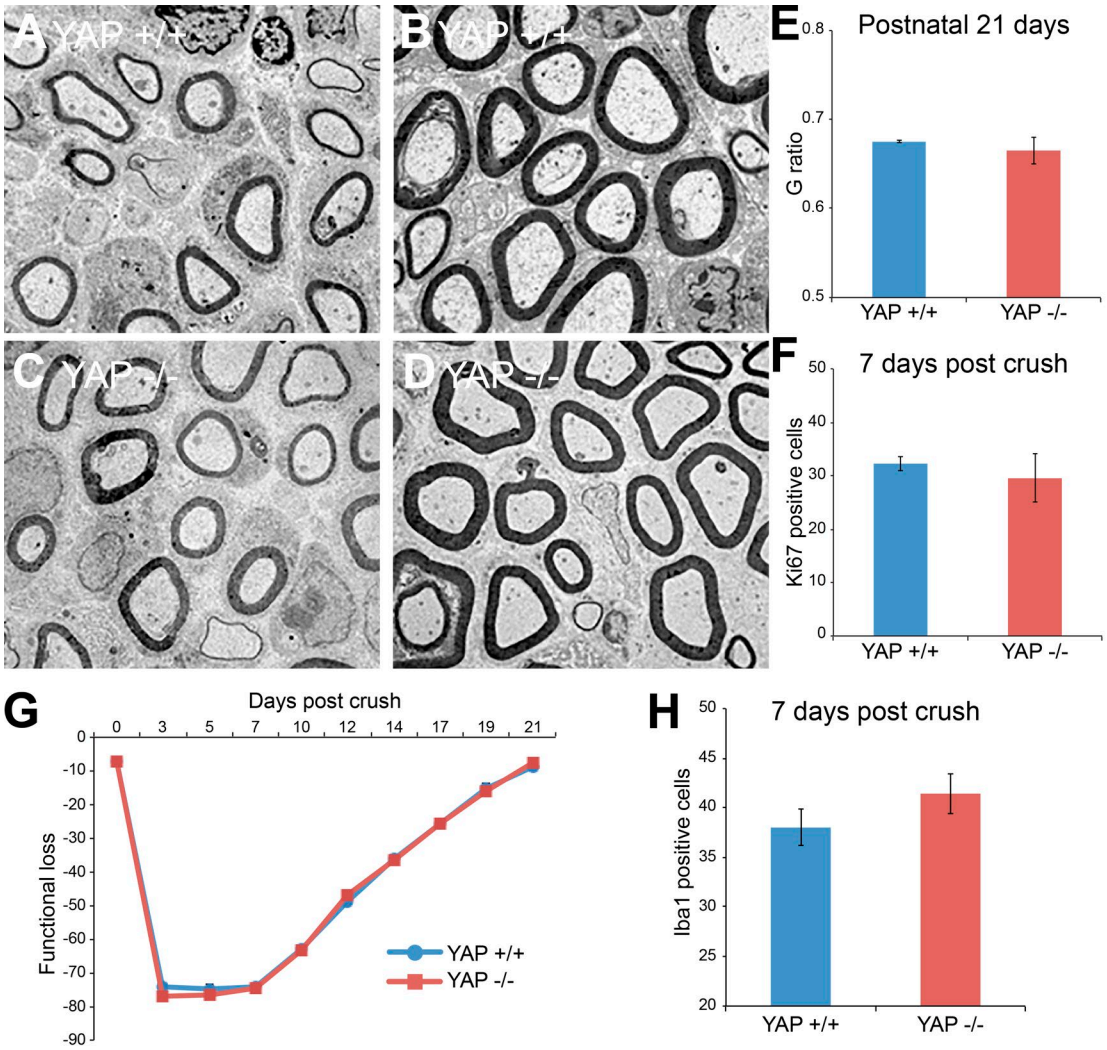

Figure S4. **Characterization of YAP single-null animals before and after injury.** (A–D) Transmission EM pictures of P6 (A and C) and P21 (B and D) sciatic nerves from control ($YAP^{+/+}$) and YAP-null ($YAP^{-/-}$) animals. (E) G ratio measurements of control and YAP-null animals at P21. *n* = 4 mice. (F) Counts of cell proliferation in distal nerves 7 d after nerve crush injury. (G) SSI measurements of control and YAP-null animals up to 21 d after nerve crush injury. (H) Numbers of Iba1-positive macrophages in the distal nerve at 7 d after nerve crush injury in control and YAP-null animals. Data are presented as means ± SEM. (F–H) *n* = 3 mice. (E–H) Two-sided two-sample Student's *t* test: P = 0.525 (E); P = 0.27 (F); P = 0.252 (H).

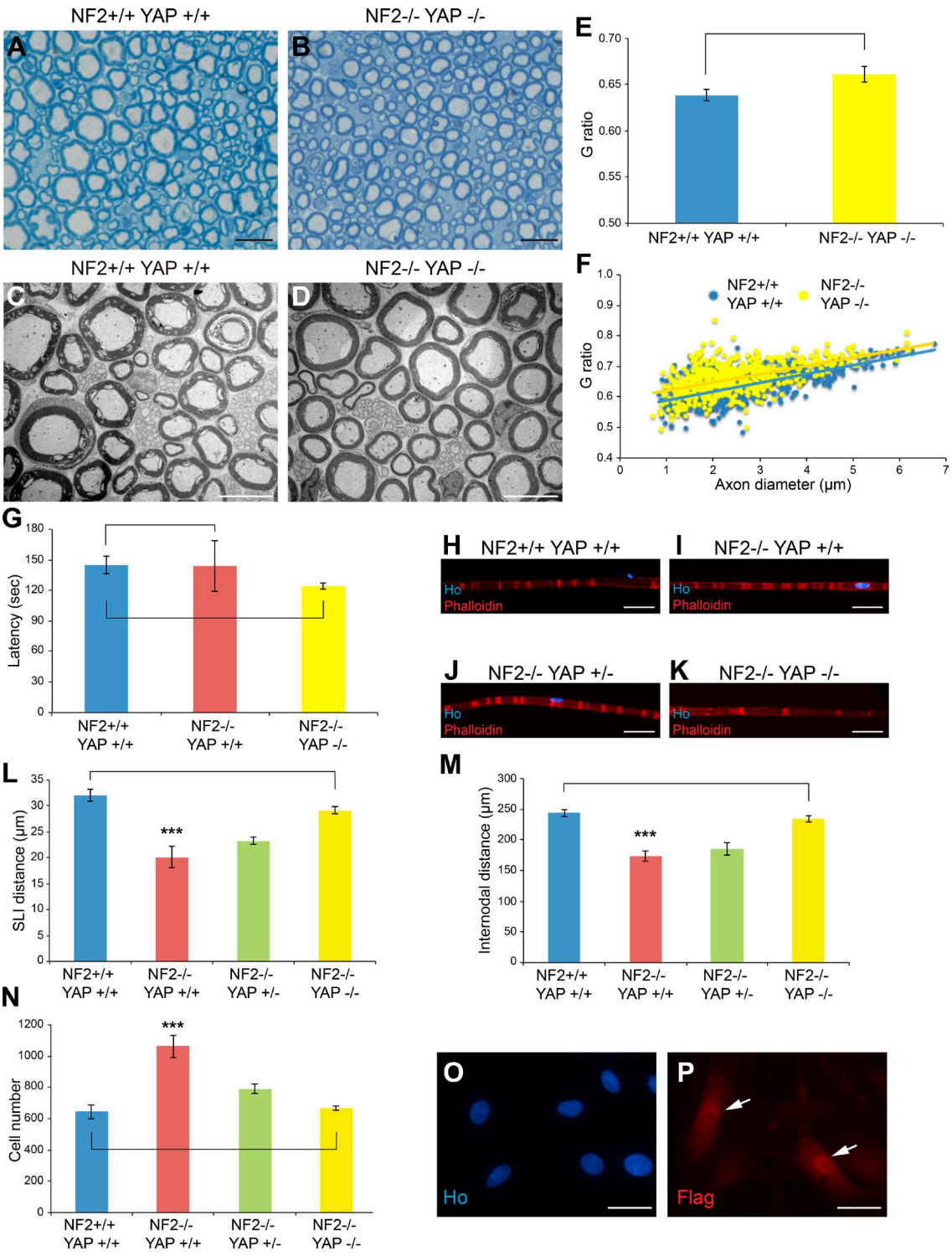

Figure S5. **Characterization of adult Merlin/YAP double-null sciatic nerves.** (A and B) Toluidine blue–stained semithin sections of adult control ($NF2^{+/+}YAP^{+/+}$) and Merlin/YAP double-null ($NF2^{-/-}YAP^{-/-}$) sciatic nerves. Bars, 10 µm. (C and D) Transmission EM images of adult control (C) and Merlin/YAP double-null (D) sciatic nerves. Bars, 5 µm. (E and F) G ratio measurements of control and Merlin/YAP-null nerves showing means (E) and scatter plots (F) of axon diameter versus G ratio. *n* = 3 mice per genotype. (G) Results of the rotarod test showing latency to fall on adult control, Merlin single-null, and Merlin/YAP double-null animals. (H–K) Phalloidin staining of teased nerve fibers of the sciatic nerve visualizing Schmidt-Lanterman incisures in control, Merlin single-null, and Merlin/YAP double-null adult nerves. Bars, 25 µm. (L–N) Loss of YAP in Merlin-null nerves normalizes the distance between adjacent Schmidt-Lanterman incisures (SLIs; L), internodal distance (M) in teased nerve fibers, and cell number (counts of Hoechst-stained nuclei in transverse cryostat sections; N) at P60. *n* = 4 mice. Data are presented as means ± SEM. (E and L–N) One-way analysis of variance with Bonferroni's multiple comparison test: *P* = 1 for $NF2^{-/-}YAP^{+/+}$ and P = 0.659 for $NF2^{-/-}YAP^{-/-}$ compared with $NF2^{+/+}YAP^{+/+}$ (E) and ***, $P \leq 0.001$ (L–N) for $NF2^{-/-}YAP^{+/+}$ compared with the other genotypes. P = 0.626 (L); P = 1 (M and N) for $NF2^{-/-}YAP^{-/-}$ compared with $NF2^{+/+}YAP^{+/+}$. (O and P) Hoechst (O) and Flag (P) immunolabeling of rat SCs expressing $YAP^{Ser127Ala}$. *n* = 3 experiments. Arrows in P indicate Flag-labeled YAP-overexpressing rat SCs showing clear cytoplasmic and nuclear localization of the $YAP^{Ser127Ala}$ protein. Bars, 10 µm. (E) Two-sided two-sample Student's *t* test: P = 0.103.